RESUMO

O trabalho que se apresenta nesta tese foi realizado âmbito do comportamento mecânico de materiais e superfícies, nomeadamente na determinação de tensões residuais induzidas por tratamentos mecânicos superficiais, como é o caso da grenalhagem de pré-tensão.

O objectivo principal do trabalho realizado foi a análise estatística dos resultados das medições obtidas com a técnica de difração de raios-X em dentes de engrenagens tratadas por grenalhagem para aferir da homogeneidade do tratamento em toda a engrenagem. Assim, no futuro, será possível diminuir o trabalho de medida necessário à análise das tensões residuais introduzidas na superfície dos dentados, tratados por este tipo de tratamento mecânico de superfícies. Estes tratamentos são usualmente usados pelos fabricantes de forma a aumentar a resistência à fadiga superficial dos dentes das engrenagens e, por essa via, aumentar o seu desempenho e tempo de vida.

Para cumprir o objectivo do trabalho, foram retirados dentes de rodas dentadas de posições distintas e as tensões residuais foram medidas por difracção de raios-X, tanto à superfície, como em profundidade.

Além disso, a microestrutura do material foi analisada em pontos equivalentes e a dureza foi medida de forma a avaliar-se a profundidade afectada pelo tratamento de grenalhagem.

Os resultados obtidos foram tratados estatisticamente através de quatro processos distintos e os resultados parecem indicar que futuramente se poderá reduzir significativamente o tempo e os custos de medida.

Este trabalho foi realizado no laboratório de análise de tensões residuais da Universidade de Kassel no âmbito de um trabalho para a indústria. No presente caso, as engrenagens analisadas foram fabricadas pela Ford e o objectivo do trabalho encomendado foi verificar a qualidade final dos tratamentos superficiais realizados

Palavras-chave: Grenalhagem, tensões residuais, Difracção de raios-X, distribuição Normal, distribuição de Weibull.

ABSTRACT

The following work was performed in the ambit of mechanical behaviour of materials and surfaces, namely in the determination of residual stresses induzed by mechanical surface treatments, such as pre-stress shot peening.

The main objective of the developed work is the statistical analyses of the results obtained by X-ray measurement in teeths from gears mechanically treated by shot peening in order to give a homogeneous treatment throughout the surface of the gear. So that, in the future, it will be possible to decrease the measurement work necessary to measure the residual stresses introduced in the material, treated by shot peening. These treatments are commonly used by the manufactures so that it is possible to increase its fatigue limit so that the material performance and life time will be also increased.

To fulfil the work objective, teeth were removed from distinct positions in the gears and the residual stresses were measured through X-ray diffraction methods in the surface and in depth. Futhermore, the microstructure and hardeness of the material were measured in equivalent points to evaluate the depth affected by shot peening.

The results obtained were statisticly treated through four different processes and they seem to inform that in the future, time and measurement costs can be significantly reduced.

This work was accomplished in the laboratory of residual stresses, in Kassel University in the ambit of a service to the industry. In this particular case, the parts were produced by Ford and the objective of the requsted work was to verify the final quality of the performed surface treatments.

Keywords Shot peening process, residual stresses, X-Ray diffraction, Normal distribution, Weibull distribution.

Index

INDEX OF FIGURES

INDEX OF TABLES

NOMENCLATURE

CHAPTHER TWO

F	Strength
σ_n	Nominal Stress
ε	Nominal Strain
E	Young's modulus
d_1	Edge lengths of the indentation rectangle
$A_{contact}$	Vickers indenter contact area
n	Number of wavelengths
Θ	Diffraction angle (theta)
d	Inter-planar spacing (perpendicular distance between adjacent parallel crystallographic planes
d_0	Inter-planar spacing (strain free)
λ	Wavelength of the X-Ray
σ_x	Stress in *x* direction
σ_y	Stress in *y* direction
σ_z	Stress in *z* direction
ε_x	Strain *x* direction
ε_y	Strain in *y* direction
ε_z	Strain in *z* direction
ν	Poisson's ratio
ϕ	Angle between a fixed direction in the sample plane and the projection in that plane of the diffracting plane normal (phi)
ψ	Angle between the sample normal and the diffracting plane normal (psi)
σ_ϕ	Single stress acting in a chosen direction

1. INTRODUCTION

Residual stresses can be defined as the stresses which remain in equilibrium in a material in the absence of any external forces. There are many stress determination methods. Some of those methods are destructive and some are nondestructive. X-ray residual stress measurement is considered as a nondestructive method. [13]

X-ray diffraction together with the other diffraction techniques of residual stress measurement uses the distance between crystallographic planes as a strain gage. The deformations cause changes in the spacing of the lattice planes from their stress free value to a new value that corresponds to the magnitude of the residual stress. Because of Poisson's ratio effect, if a tensile stress is applied, the lattice spacing will increase for planes perpendicular to the stress direction, and decrease for planes parallel to the stress direction. This new spacing will be the same in any similarly oriented planes, with respect to the applied stress. Therefore the method can only be applied to crystalline, polycrystalline and semi-crystalline materials. The diffraction angle, 2θ, is measured experimentally and then the lattice spacing is calculated from the diffraction angle, and the known x-ray wavelength using Bragg's Law. Once the d-spacing values are known, they can be plotted versus $\sin^2\psi$, (ψ is the tilt angle).

In this paper, stress measurement of the samples that exhibit a linear behaviour as in the case of a homogenous isotropic sample in a biaxial stress state is included.

Furthermore, statistical tests were made to the result of the measurement to determine if the distribution of the latter, such as any other, can be approximated by a normal distribution or in the case of the multiple measurements, to a Weibull distribution.

2. STATE OF THE ART

2.1. Origin and nature of residual stresses

By definition, it is possible to say that residual stresses are static multiaxial stresses that exist in an isolated system that is in mechanical equilibrium. In general, every homogeneous deformation introduced in a structure leads to the formation of residual stresses. These stresses can come from macro, micro or submicroscopic deformations and that is why they are divided in three main groups. The first order residual stresses reach until several grains in the material and are homogeneous. The pre-stresses that are resultant from surface treatments, are inserted in this group. The second order residual stresses are homogeneous only in small domains of the material (one grain). These are due to the anisotropy of the grains, which haven't got the same crystalline orientation or due to the presence of different phases that constitute the material within the material (different mechanical properties or different dilation coefficients). Finally the third order of residual stresses, that are not homogeneous in some inter-atomical distances which are related to every lattice imperfection such as dislocations, grain boundary and precipitates. In this situation the state of real stress is an overlapping of these stress states. Normally, there is no kind of distinction between second and third order stresses and these are denominated microstresses and the first order, are called macrostresses. [1]

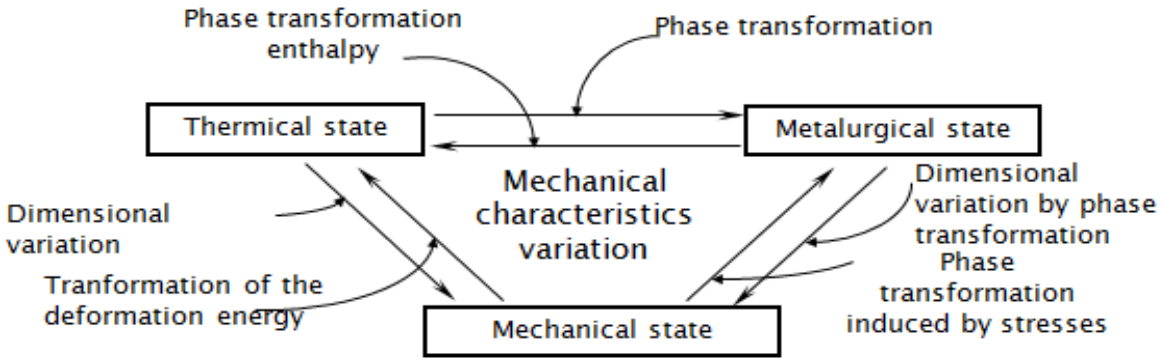

Figure 1 - Origin of the residual stresses.

2.2. Surface Treatments

The life time of mechanical components that are utilised under in different situations that can be related to corrosion, fatigue and wear, depends on the properties of the superficial layers of the materials that the components are made of.

The main objective of the surface treatments is to introduce compressive residual stresses in the superficial layers and increase its strength for the situations that it is used. The origin of these stresses is the heterogeneity of the deformation, provienient of an irreversible elongation of those layers, which is incompatible with the rest of the part that can't be deformable or it deforms according to a different law.

These local deformations are created inside the material due to thermal, mechanical and metallurgical effects. These factors can act together or independently, making complex the prevision of the value of the induced residual stresses and their evolution during use, according to different treatments. Based on the main effect of the surface treatment, it is possible to divide them into three main groups: mechanical, thermical and thermochemical surface treatments.

Mechanical treatments use local plastic deformation (not homogeneous) to introduce compressive residual stresses. Shot peening, hammering, deep rolling and mechanical polishing are some examples. Thermal surface treatments are based on the dialation of the material, through a possible phase change and local plastic deformation. When associated, these treatments can increase the hardness of the material. These treatments can act on the whole section or only in a heated surface layer, acting in different times and in different zones of the surface. In this group it is possible to introduce the quenching treatment with or without phase transformation. In the group of thermochemical treatments it is possible to refer the case hardening by atoms diffusion (carbon and nitrogene) in the material superficial layer in order to improve the quenching properties, increase hardness and strength and then create residual compressive stresses. Case hardening, carbonitriding and carburizing are some examples of thermo chemical treatments.

These last two surface treatments can be followed by a mechanical treatment, such as shot peening in order to obtain a better combination between superficial hardening and compressive residual stresses. [14]

In this work, it will be given more relevance to the shot peening surface treatment process and how it affects the material.

2.2.1. Pre-Stress Shot peening

Pre-stress shot peening main objective is the introduction of compressive residual stresses in the superficial layers of the material and improve its resistance to fatige.

The procedure uses pneumatical machinery to project onto the deirsble surface, small spheres with an elevated hardness (steel, glass, ceramic), with diameters between 0,1 and 2 mm, with a speed between 20 and 120 m/s and contact pressures around 1500 MPa are made by each sphere during 1μs. The impact causes plastic deformation of the superficial layer which corresponds to an elongation of the superficial fibers of the treated material. The under layers are less deformed and they limit the superficial layer elongation then making it to stay in a compressive state.

Modifying the shot peening parameters (nature, hardness, shot diameter, impact speed and impact angle) it is possible to impose a controllated hardening of the surface until a depth of 0,1 to 1 mm in order to obtain the desirable hardness increase and a compressive residual stress value. [15]

These parameters should be adjusted depending on the hardness of the material to treat. The mechanical characteristics of the material influence the value, distribution and stability of these stresses. Tempering treatments made after shot peening have a benefical effect on stabilizing the compressive residual stresses of the material. The temperature, however, must be controlled (200-250ºC) so that afterwards the residual stresses created before, do not relax. [1]

2.2.2. Shot peening effect

Fretting fatigue induces damage at or near contact surfaces, which is caused by micro-slip of the contacting components subjected to cyclic load as well as contact fatigue. This result in a reduction of fatigue life compared to conventional fatigue with no contacting components, due to an increased axial and shear stresses at the contact interference [1-3]. In many cases, components subjected to fatigue

loading conditions are given surface treatments to enhance their fatigue resistance, and shot peening is the most widely used treatment among them [4, 5]. Shot peening involves blasting of spherical balls of a hard material against the surface of the component. This process induces a residual compressive stress on the surface and a compensating residual tensile stress away from the surface since the shot peened surface layer tries to expand while the region below the surface resists the expansion. The residual compressive stress on the surface can prevent crack initiation and propagation as well as close pre-existing cracks when they are within the depth of the compressive zone. Many studies have demonstrated the increased fatigue life of shot peened material components as compared to unpeened components under various fatigue situations. [6, 7].

Residual stresses can relax during service via mechanical and thermal processes. As the relaxation of residual stresses implies the reduction of beneficial effect of shot peening on fatigue behaviour, there have been several investigations about the relaxation behaviour of residual stresses under only thermal exposure, static loading, cyclic loading and thermo mechanical loading conditions. Mechanical relaxation of residual stresses occurs when the superposition of applied stress and residual stress reach the maximum yield strength of the material. Thermal relaxation of residual stress is a thermal recovery process in which elevated temperature accelerates a rapid annihilation of crystalline defects. [1]

2.2.3. Dang Van's fatigue criterion

Using some criterions for high cyclicing multiaxial fatigue, as the case of DangVan's fatigue criterion, it is possible to clear show the importance of the mechanical surface treatments, such as shot-peening. Before detailing the calibration of the Dang Van locus, an outline of the practical application of this criterion will be given. The basis of the following relationships is the application of the elastic shakedown principles at the mesoscopic scale, which will be shortly explained.

The dang Van criterion can be expressed by the following equation:

$$\tau_{\max}(t) + a_{dv}\sigma_H(t) = \tau_W \quad (1)$$

with a_{dv} being the constant of the material to be determined, τ_W the fatigue limit in reversed torsion, $\sigma_H(t)$ the instantaneous hydrostatic component of the stress tensor and $\tau_{\max}(t)$ the instantaneous value of the Tresca shear stress.

$$\tau_{\max} = \frac{\hat{s}_I(t) - \hat{s}_{III}(t)}{2} \tag{2}$$

Evaluated over a symmetrised stress deviator, which is obtained by subtracting from the stress deviator:

$$s_{ij}(t) = \sigma_{ij}(t) - \delta_{ij}\sigma_H(t) \tag{3}$$

a constant tensor, $s_{ij}(t)$,

$$\hat{s}_{ij}(t) = s_{ij}(t) - s_{ij,m} \tag{4}$$

The constant tensor, $s_{ij,m}$, is defined by the relationship:

$$\max_t \left[\left(s_{ij}(t) - s_{ij,m} \right) \left(s_{ij}(t) - s_{ij,m} \right) \right] = \min_{s'_{ij}} \max_t \left[\left(s_{ij}(t) - s'_{ij} \right) \left(s_{ij}(t) - s'_{ij} \right) \right] \tag{5}$$

The constant tensor, $s_{ij,m}$, may be regarded as the part of the stress deviator, which has no influence on the fatigue crack nucleation, and therefore, is eliminated through the minimization process of equation 5. One of the consequences of this method is the correct prediction of the absence of any effect of a mean shear stress upon the torsional fatigue limit.

In Dang Van initial proposal, the existence of the constant stress deviator, $s_{ij,m}$, is justified by the assumption that the stress deviator defined by equation 4 is the stress state found at the grain scale. Close to the fatigue limit, some unfavourably oriented grains may still undergo cyclic plasticity, although the macroscopic behaviour appears elastic. For crack nucleation to be avoided, these grains necessarily have to reach an elastic shakedown state. The presence of the residual stress deviator defined by equation 5, allows fulfilment of this condition.

Defined at the microscopic scale, these residual stresses are different from those developing as a consequence of a structural elastic shakedown. In this case, the minimization procedure of equation 5 would not be enough and the evaluation of residual stresses would require the classical procedures of the theory of plasticity.

If the macroscopic stress state exceed the yield limit, because of the assumption of an elastic behaviour of the crystalline aggregate surrounding the unfavourably oriented grains, the Dang Van criterion would not be applicable, unless the material shakes down to the elastic state also at the macroscopic level. For this reason, Dang Van criterion can be applied to some rolling contact fatigue problems, provided that the contact conditions allow for the elastic shakedown of the material subjected to contact stresses.

Going back to equation 1, because of the symmetrisation of the stress deviator, the term $\tau_{\max}(t)$ alone cannot account for the effect of normal stresses upon the fatigue limit. For this reason, the effect of a mean normal stress upon fatigue limits in bending and torsion is taken into account by introducing in equation 1, the term $a_{dv}\sigma_H(t)$. This term represents the effect of the hydrostatic stress on crack nucleation and it can also be demonstrated that macroscopic and mesoscopic hydrostatic stresses are the same. [9]

If residual stresses are superimposed on the applied stresses, the term $\tau_{\max}(t)$ is not altered because of the minimization process of equation 5. However, the term $a_{dv}\sigma_H(t)$ is modified by the presence of residual stresses throught the hydrostatic part of the residual stress tensor $\sigma_{H,res}$, and therefore equation 1 becomes:

$$\tau_{\max}(t) + a_{dv}\left[\sigma_H(t) + \sigma_{H,res}\right] = \tau_W \tag{6}$$

The constant a_{dv} appearing in the expression of the Dang Van criterion is usually calibrated with two fatigue tests, pure bending (or tension-compression) and pure torsion. In the space constituted by the symmetrized shear ($\tau_{\max}$) and the hydrostatic stress (σ_H), reversed torsion and alternating bending are represented by a vertical line segment and a V-shape curve, respectively. As shown schematically in figure 2, the fatigue locus is then assumed as the straight line tangent to these two lines, with a constant slope given by the following expression:

$$a_{dv} = 3\left(\frac{\tau_w}{\sigma_w} - \frac{1}{2}\right) \tag{7}$$

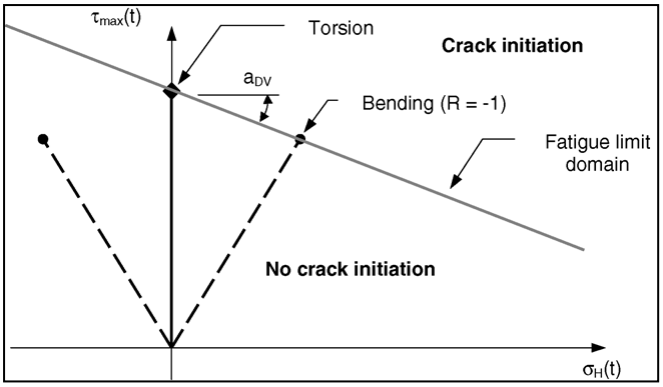

Figure 2- The Dan Van diagram: a scheme of typical calibration with bending and torsion fatigue test.

Peridas and Hill [11], pointed out the importance of using more than these two tests. The first aim of their proposal is to obtain a more accurate fatigue test domain. In fact, as the limit line is tangent to the paths corresponding to pure bending and torsion tests, which are close to each other, small errors have a profound effect on the slope of the locus line. The second and maybe more important aim of their proposal is to confirm, on the basis of a more extended amount of data coming from experiments, the suitability of the Dang Van criterion to reproduce simple experimental cases. [8]

DangVan has proposed an endurance limit criterion based on the concept of microstresses within a critical volume of the material. This model arises from the observation that fatigue crack nucleation is a local process and begins in grains that have undergone plastic deformation and form characteristic slip bands. It is hypothesized that because cracks usually nucleate in intragranular slip bands, the microscopic shear stress on a grain must be an important parameter. In the same way, it is reasoned that the microscopic shear stress on a grain must be an important parameter. In the same way, it is reasoned that the microscopic hydrostatic stress will influence the opening ofthese cracks or slip bands. The simplest failure criterion involving these two variables is a linear combination

$$\tau(t) + a\sigma_H = b \tag{8}$$

Where $\tau(t)$ and $\sigma_h(t)$ are instantaneous microscopic shear stress and hydrostatic stress and a and b are constants. The constant b is the fatigue strength determined from a torsion test and a is related to the sensitivity of the material to hydrostatic stress.

The microscopic stresses and strains within critical grains are different from the macroscopic stresses and strains commonly computed for fatigue analysis. Two size scales have been distinguished in the model:

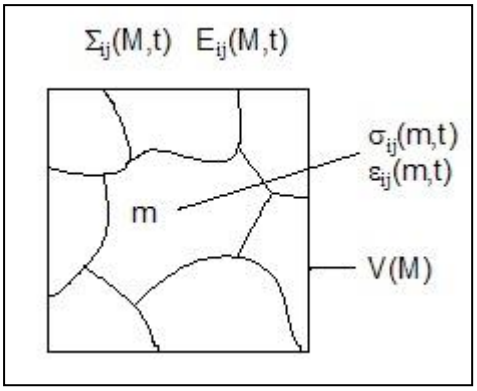

Figure 3 – Macroscopic and microscopic scales.

- A macroscopic scale is characterized by an elementary volume V(M) surrounding a point where the fatigue analysis is to be performed. This size scale is on the order of a strain gage or FEM element. This is the scale considered by engineers and is the same as local stresses and strains as defined in the "local strain" approach to fatigue analysis. Macroscopic stresses are denoted $\Sigma(M,t)$ and strains $E(M,t)$. They are both functions of position within the structure, M, and time, *t*.
- A microstructural scale on the order of a grain or other suitable microstructural unit corresponding to a subdivision of V(M). Microscopic stresses $\sigma(m,t)$ and strains $\varepsilon(m,t)$ are related but not equal to $\Sigma(M,t)$ and $E(M,t)$.

At the microstructural scale, a material is neither isotropic nor homogenous and the values $\sigma(m,t)$ and $\varepsilon(m,t)$ will be different from the local macroscopic variables $\Sigma(M,t)$ and $E(M,t)$. Plastic shear deformation of the grains with the most severe orientations is constrained due to the elastic behavior of neighboring grains having less severe orientations. If fatigue failure is to be avoided, the stresses and strains in the critically oriented grains must stabilize by the process of elastic shakedown and thus prevent crack growth to the neighbouring grain.

Computation of the elastic shakedown state under multiaxial loading is illustrated with the help of the following figure. The initial elastic domain of the critical volume of material is illustrated by the circle C_o, with center at $O_o$and radius R_o. As loading progresses the material undergoes combined kinematic and isotropic hardening as the centre of the yield surface translates and the radius of the surface increases. After several repetitions of the load path, a stable domain C_L with center $O_L$and radius R_L will evolve. The stable path is characterized by the smallest circle, C_L that completely encloses the load path. The stabilized residual stress tensor, r*, corresponds to O_L - O_o. For tension-torsion loading the domain C_L corresponds to a circle in $\sqrt{3}\tau - \sigma$ stress space but in the general loading case where all six stress components change, the domain C_L is a six dimensional hypersphere.

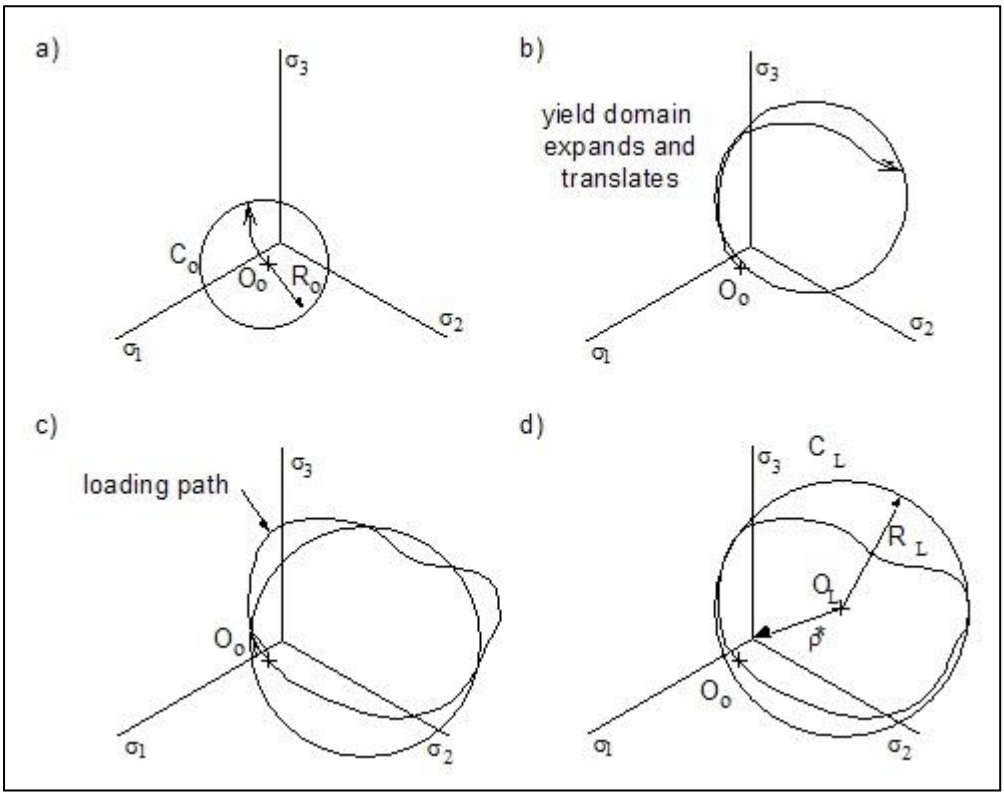

Figure 4 – Elastic shakedown under multiaxial loading

Computationally, a combined isotropic and kinematic cyclic plasticity model is used to obtain an estimate of the microscopic stresses acting on the critical grain. Evaluation of the microscopic residual stresses that arise from the combined

isotropic and kinematic hardening tensor r* is a critical part of this model and distinguishes it from the other stress based models.

The resulting microscopic stresses, σ_{ij}, are obtained from the macroscopic stress microscopic residual stresses

$$\sigma_{ij}(t) = \sum_{ij}(t) + dev\rho^* \tag{9}$$

where dev ρ* is the deviatory part of the stabilized residual stress tensor.

The microscopic shear stress which is used in the failure criterion is computed from the microscopic principal stresses at every point in the loading cycle using the Tresca maximum shear stress theory.

$$\tau(t) = \frac{1}{2}\left[\sigma_1(t) - \sigma_3(t)\right] \tag{10}$$

The failure criterion can then be expressed as combinations of t(*t*) and hydrostatic stress. The constants *a* and *b* are obtained from materials tests at two different stress states. A loading path that remains within the two bounding failure lines is expected to have infinite life while any path that extends outside the damage line will have fatigue failures because microscopic plastic strains occur.

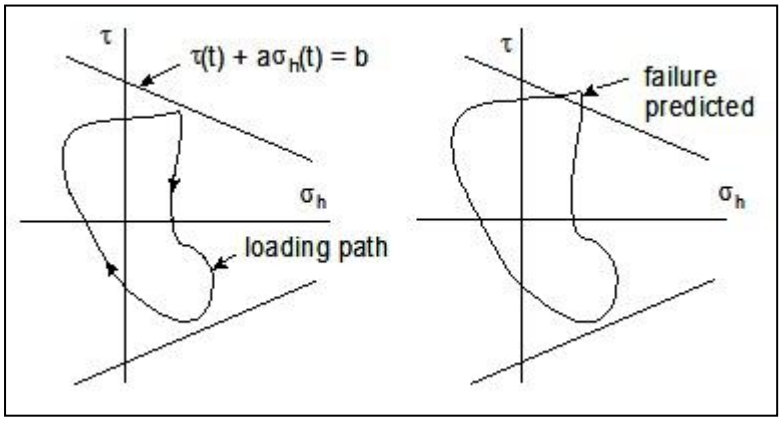

Figure 5 – Dang Van criteria.

The Dang Van criterion is intended as a method of predicting the endurance limit under complex loading situations. Unlike the other methods, the output from the analysis is always expressed as a safety factor not a fatigue life. The consequence of the surface treatments, such as shot peening, is the backing of the area that defines the safe fatigue zone (increasing resistance of the material by hardening) for one

side, for the other side, the value of the hydrostatic stress decreases, making the loading path move to the left. Which is also the same as saying that the residual stresses only vary the medium stresses are the only ones that vary, in other words, the hydrostatic component of the stress tensor. The improvement that is obtained in the resistance to the fatigue is important to be referred. It is computed as: [9]

$$n = \frac{b}{\left(\tau(t) + a\sigma_H(t)\right)_{\max}} \tag{11}$$

2.3. X-Ray Diffraction

There are many techniques to measure residual stresses in materials, among them there is the X-Ray diffraction technique which has a particular place because it enables a non destructive evaluation of surface stress, essential to estimate the fatigue life of mechanical parts and delivers real-time analysis of stress evolution. [12]

2.3.1. Principle of X-Ray Stress Measurement and Bragg's Law

When a monochromatic X-Ray beam irradiates a solid material, it is scattered by the atoms composing the material. For a perfect crystalline material, atoms are packed regularly in a three dimensional periodic lattice, as it is possible to be seen in th figure 2.1. The distance between the crystallographic planes is characteristic of each material in a given environment. Because the atoms are packed in a regular distribution, the scattered waves lead to interferences similar to visible light diffraction by an optical diffraction pattern. The intensities of the scattered waves sum up in a constructive interference when the condition

$$2d\sin(\Theta) = n\lambda \tag{12}$$

is fulfilled, where d is the distance between the diffracting lattice planes, Θ is the angle between the incident beam and the diffracting planes, λ is the X-ray wave length and n is an integer. If this condition, called Bragg's Law, the diffracted beam and the incident beam are symmetrical in relation to the lattice planes normal. An

infinity of crystallographic planes can be defined, but only few of them lead to a diffraction pattern with a detectable intensity, due to physical reasons. [12]

When a beam irradiates the surface of a crystalline material, it is constructively scattered only if it meets lattice planes oriented to fulfil Bragg's law. If the material is composed of many grains randomly oriented, there is always a group of them suitably oriented to produce a diffracted beam, as can be seem in the following figure. [12]

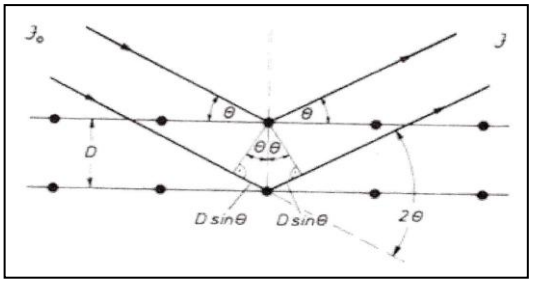

Figure 6 - Schematic representation of Bragg's interference.

2.3.2. Determination of lattice strain by X-ray diffraction

When the crystalline material is irradiated by a monochromatic X-ray beam with a certain λ wavelength of the same magnitude as the lattice spacing, an increased scattering intensity can be observed in the neighbouring of a few 2Θ angle values. This increased intensity, called diffraction peaks, comes from a constructive interference of the X photons scattered by the atoms of the crystal. Their position 2Θ depends on λ and on the lattice spacing d through the Bragg's law,

$$2d\sin(\Theta) = n\lambda \text{, where } n \text{ is an integer.}$$

So, the lattice spacing of crystallographic planes *{hkl}* on which the measurement is performed is related to the position Θ of the diffraction peak through Bragg's law. A homogeneous elastic deformation of the crystal will result in a change in the spacing d_{hkl}, because the planes tend to get closer when in a compressive state and to separate when in a tensile state. Therefore, the crystal lattice itself and the family of planes can be used as a strain gage (for the elastic part of the deformation). Then the strain can be calculated from d_{hkl} and thus from Θ, as can be see in the following figure. [12]

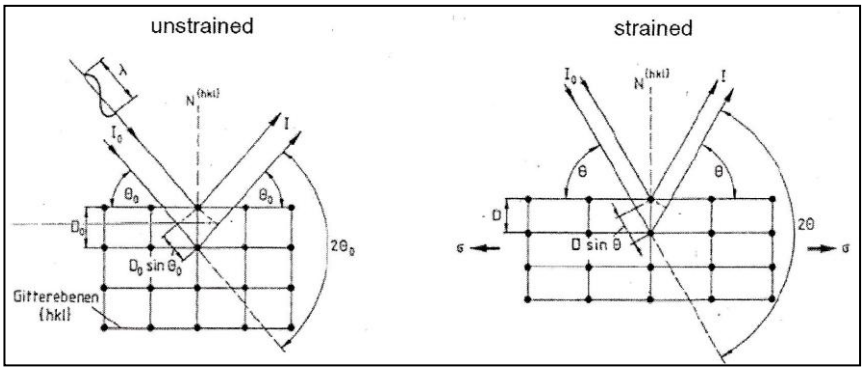

Figure 7 - Unstrained and strained lattice, corresponding to changes in the angles.

Then the measured stress can be express in relation to a reference state of the material called stress free state. In this state, the lattice spacing of planes *{hkl}* equals to d_0 which is a function of the lattice parameters of the stress free crystal. Then, because of an elastic deformation, the lattice spacing will be equal to *d*. The conventional stress can be expressed as:

$$\varepsilon = \frac{d - d_0}{d_0} \tag{13}$$

using Bragg's law:

$$\varepsilon = \frac{\sin\Theta_0}{\sin\Theta} - 1 \tag{14}$$

So, the elastic strain of the crystal can therefore be obtained from the position of the diffraction peaks recorded before and after deformation. For greater accuracy the rational stress can be used:

$$\varepsilon = \ln\left(\frac{d}{d_0}\right) = \ln\left(\frac{\sin\Theta_0}{\sin\Theta}\right) \tag{15}$$

However for small deformations (<0,2%), the rational stress is very close to conventional stress.

An approximation of the rational strain can be obtained with a series of expansions of ln(x) truncated after first order:

$$\ln(x) = \left(\frac{x-1}{x}\right) + \frac{1}{2}\left(\frac{x-1}{x}\right)^2 + \ldots \tag{16}$$

If $\frac{d}{d_0}$ is substituted for x, then:

$$\varepsilon = 1 - \left(\frac{\sin \Theta}{\sin \Theta_0} \right) = -\cot g \Theta_0 . \Delta\Theta \tag{17}$$

Though these equations are mathematically very different, they lead to very close values of the strain because X-ray diffraction is only sensitive to elastic (small) deformation. [12]

2.3.3. Determination of stress by X-ray diffraction

By using Bragg's Law it is possible to measure the lattice strains within the range near the surface and the stress that produce these strains can also be calculated.

The equation of Hooke's Law, the classical law of elasticity, presents the relation between stress and strain according the following equation:

$$\sigma_y = E\varepsilon_y \tag{18}$$

Knowing that a measured stress state can be often interpreted as a plane stress state and the stresses are biaxial, then we have [8]:

$$\varepsilon_x = \varepsilon_y = -\nu\varepsilon_z = \frac{-\nu\sigma_y}{E} \tag{19}$$

$$\varepsilon_z = -\nu(\varepsilon_x + \varepsilon_y) = \frac{-\nu}{E}\left(\sigma_x + \sigma_y\right) \tag{20}$$

2.3.4. The $\sin^2\psi$ – Method

One method used to calculate the stress by X-Ray diffraction is the $\sin^2\psi$. When this method is used, the X-ray diffraction measurements are performed at different psi-angles. In each of these different psi-angles, a measurement of the 2-theta peak position, or inter-planar spacing, is performed. The relations between the stresses and deformations can be obtained through solids mechanics:

$$\varepsilon_{\phi\varphi} = \frac{1+\upsilon_{hkl}}{E_{hkl}}\left(\sigma_{11}\cos^2\phi + \sigma_{12} sen2\phi + \sigma_{22} sen^2\phi\right) sen^2\varphi - \frac{\upsilon_{hkl}}{E_{hkl}}\left(\sigma_{11} + \sigma_{22}\right) \tag{21}$$

being E and υ the Young's module and the Poisson's coefficient respectively, and and where E_{hkl} and υ_{hkl} are different from those normally used in mechanical rehearsals and due to the X-ray selectivity, it only analyses the crystalline deformation that is in a favourable crystallographic plane orientation. It is usual to use the crystallographic constants:

$$S_1(hkl) = -\frac{\upsilon_{hkl}}{E_{hkl}} \tag{22}$$

$$\frac{1}{2}S_2(hkl) = \frac{1+\upsilon_{hkl}}{E_{hkl}} \tag{23}$$

These constants can be determined experimentally or through the elastic constants of the monocrystal. Replacing the value of these constants in equation (21), it is possible to obtain the following equation:

$$\varepsilon_{\phi\varphi} = \frac{1}{2}S_2\sigma_\phi sen^2\varphi + S_1 tr(\sigma) \tag{24}$$

According to this equation, the evolution of the crystallographic deformation $\varepsilon_{\phi\varphi}$, is a straight line with a slope proportional to the normal stress σ_ϕ with ordinate in the origin which is proportional to the stress tensor and is normally named by $sen^2\varphi$ law. The stress σ_ϕ can be them determined by making two data acquisitions in the diffraction peak to different φ angles, keeping constant the ϕ angles. The average value of σ_ϕ can be determined through the line slope as long as the value of $\frac{1}{2}S_2$ is known.[12]

2.3.5. The Integral Width

The integral width is characterized by the hardening or softening of the material condition. It is related to the dislocation density and gives qualitative information about the occurrence of plastic deformation. By definition, it represents the width of a rectangle with the height of the reflected intensity. The rectangle area is equal to the one under the reflected peak as in figure 8.

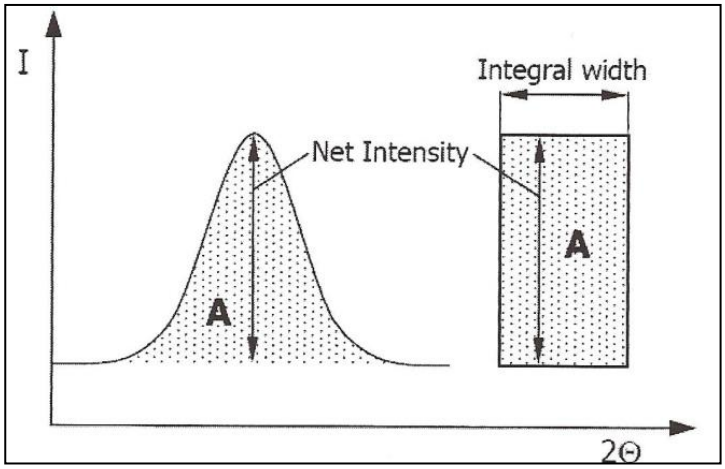

Figure 8 - Schematic representation of the integral width.

2.4. Statistical Tests

The statistical tests corresponding to the results of the performed measurements were obtained using two different distributions: a Normal distribution and a Weibull distribution.

2.4.1. Normal Distribution

The normal distribution or Gaussian distribution is a continuous probability distribution that is used as a first approximation to describe real valued random variables that tend to cluster around a single mean value. The graphic associated to this distribution is bell shaped and is known as the Gaussian Function or bell curve, given by this equation.

$$f(x) = \frac{1}{\sqrt{2\pi\sigma^2}} e^{-\frac{(x-\mu)^2}{2\sigma^2}} \tag{25}$$

where μ is the mean value (location of the peak) and σ^2 is the variance, which measures the width of the distribution. The distribution with $\mu = 0$ and $\sigma^2 = 1$, is called a standard normal distribution. The mean value is given by the equation 26 and the standard deviation is given by equation 27, in which *N*, is the sample size:

$$\sum_{i=1}^{N} \frac{f(x)}{i} \tag{26}$$

$$\sigma = \sqrt{\frac{1}{N}\sum_{i=1}^{N}(x_i - \bar{x})^2} \tag{27}$$

The normal distribution is the most prominent probability distribution in statistics. The two main reasons for this is that, first, this distribution is very tractable analytically and there is a large number of results involving this method that can be derived in a explicit form. Second, this distribution arises as the outcome of the central limit theorem, which states that under mild conditions, the sum of a large number of random variables has a approximately normal distribution. And finally, its shape, a bell-shape, makes it a convenient choice for modelling a large variety of random variables encountered in practice.

2.4.1.1. Probabilty Density Function

The probability density function of a random variable describes the possibility of this variable to occur in a certain point.

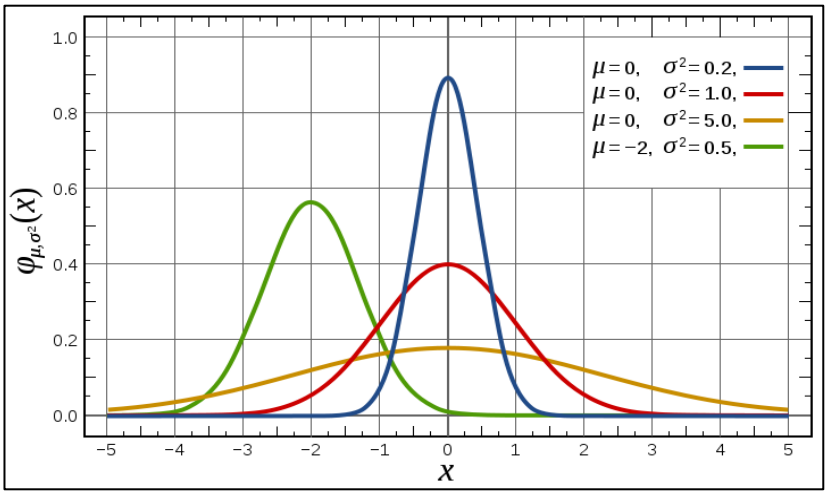

Figure 9 - Probability density function and in red the standart normal distribution.

2.4.1.2. Cumulative distribution function

The cumulative density function of a random variable describes the probability distribution of a random variable will be found at a value less than or equal to x.

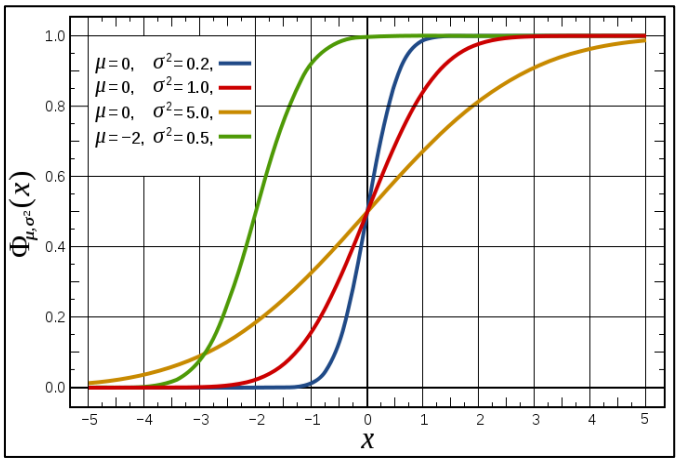

Figure 10 - Cumulative density function for the normal distribution.

2.4.2. Log-Normal Distribution

The Log-Normal distribution is a probability distribution in which its logarithm is normally distributed. A random variable X has log-normal distribution when its logarithm $Y = \log(X)$, has a normal distribution.

The probability density function, expected value and variance are given in the same order in the equations below.

$$f(x,\mu,\sigma) = \frac{1}{x\sigma\sqrt{2\pi}} e^{\left(-\frac{(\ln(x)-\mu)^2}{2\sigma^2}\right)} \tag{28}$$

$$E(X) = E\left(\exp(Y)\right) = \exp\left(E(Y) + 0,5\,\mathrm{var}(Y)\right) \tag{29}$$

$$\mathrm{var}(X) = \exp\left(2E(Y) + \mathrm{var}(Y)\right)\left(\exp(\mathrm{var}(Y)) - 1\right) \tag{30}$$

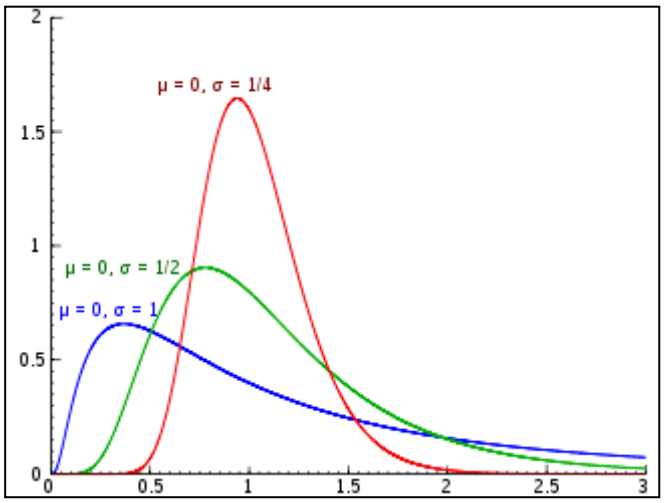

Figure 11 - Probability density function of a log-normal distribution.

2.4.3. Weibull Distribution

The Weibull distribution is a continuous probability distribution that is widely used for matching field data, due to its versatility and the fact that the Weibull probability density function can assume different shapes based on the parameter (beta factor) values.

This kind of distribution is more commonlly used in survival analyses, reliability engineering and failure analyses and in extreme value theory among others.

This distribution has got three characteristical parameters: scale parameter (η), shape parameter (β) and a postion parameter (γ).

The cumulative distribution function for a Weibull distribution is given by the mathematical expression:

$$F(t) = 1 - e^{-\left(\frac{t-\gamma}{\eta}\right)^{\beta}} \tag{31}$$

2.4.4. Calculation of the Weibull parameters

It is easy when there are data to proceed to a Weilbull graphic analysis, but how it is possible do it without having the graphic to help? Concerning the Weilbull Law, there are three important parameters to consider:

Concerning the Weilbull Law, there are three important parameters to consider:

- γ, the location parameter;
- β, the shape parameter affects the shape of the distribution rather than shifting, shrinking or stretching the distribution;
- η, the scale parameter, affects the way that the distribution is spread. The larger the scale, more spread out is the distribution.

The function density of probability associated to the Weibull Law is the following equation:

$$f(t)=\frac{\beta}{\eta}\left(\frac{t-\gamma}{\eta}\right)^{\beta-1} e^{-\left(\frac{t-\gamma}{\eta}\right)^{\beta}} \tag{32}$$

By applying an integer to this equation, we will obtain:

$$F(t)=1-e^{-\left(\frac{t-\gamma}{\eta}\right)^{\beta}}=1-\frac{1}{e^{\left(\frac{t-\gamma}{\eta}\right)^{\beta}}} \tag{33}$$

From equation number (31),

$$R(t)=1-F(t)=e^{-\left(\frac{t-\gamma}{\eta}\right)^{\beta}} \tag{34}$$

Combining equations (33) and (34), it is possible to deduce the final equation represented:

$$F(t)=1-e^{-\left(\frac{t-\gamma}{\eta}\right)^{\beta}}=1-\frac{1}{e^{\left(\frac{t-\gamma}{\eta}\right)^{\beta}}}$$

$$R(t)=1-F(t)=1-1+\frac{1}{e^{\left(\frac{t-\gamma}{\eta}\right)^{\beta}}}\Rightarrow$$

$$\Rightarrow R(t)=\frac{1}{e^{\left(\frac{t-\gamma}{\eta}\right)^{\beta}}} \Leftrightarrow \frac{1}{R(t)}=e^{\left(\frac{t-\gamma}{\eta}\right)^{\beta}} \tag{35}$$

By applying the logarithm:

$$\ln\left(\frac{1}{R(t)}\right)=\left(\frac{t-\gamma}{\eta}\right)^{\beta} \tag{36}$$

Again:

$$\ln\left(l\,n\left(\frac{1}{R(t)}\right)\right)=\beta\ln(t-\gamma)-\ln(\eta) \tag{38}$$

To $\gamma=0$:

$$\ln\left(l\,n\left(\frac{1}{R(t)}\right)\right)=\beta\ln(t)-\beta\ln(\eta) \tag{39}$$

In terms of graphical language, equation (31) corresponds to the simple expression of a line:

$$y=\beta x+b \tag{40}$$

in which β, corresponds to the tilt of the line, usually expressed by m.

After havin all these values, it is necessary to trace a line which corresponding equation must be of the type:

$$y=ax+b \tag{41}$$

in a graphic with the function,

$$\ln\left(\frac{1}{R(t)}\right)=f(t) \tag{42}$$

where $R(t)=1-F(t)$ and $t=\sigma^{RS}$.

The tilt of the line will be directly proporcional to β. So $a=\beta$. The intersection with the coordinates allows to determine η. So:

$$\begin{aligned} &b=-\beta\ln(\eta)\Rightarrow \\ &\Rightarrow \eta=e^{-\frac{b}{\beta}} \end{aligned} \tag{43}$$

If γ can not be neglected, equation (38) should be used instead, modifying the γ value until the best fit was obtained.

2.4.5. Exponencial distribution

Exponencial distribution is a family of continuous probability distributions that describe the time between events in a Poisson process; this means that is a process in which events occur continuously and independently at a constant average rate. The expressions for the probability density function, mean value or expected value and variance are the following:

$$f(x,\lambda)=\begin{cases}\lambda e^{-\lambda x}, x\geq 0\\ 0, x<0\end{cases} \tag{44}$$

$$E[X]=\frac{1}{\lambda} \tag{45}$$

$$\text{var}[X]=\frac{1}{\lambda^2} \tag{46}$$

Being λ, a rate parameter.

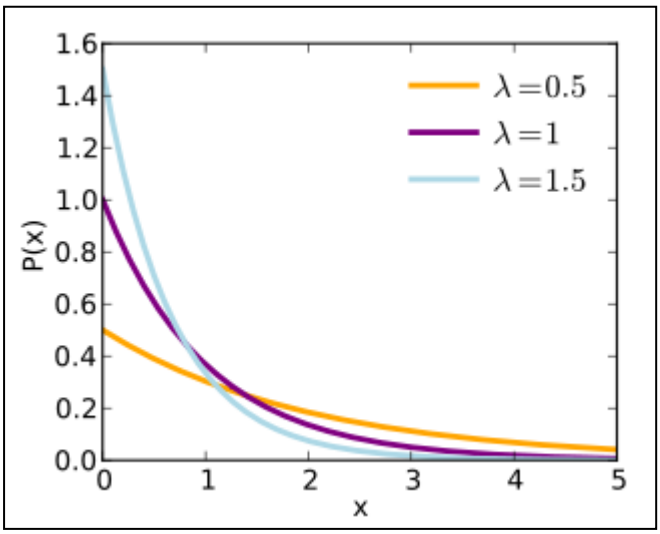

Figure 12 - Probability density function of an exponencial distribution.

3. MATERIAL, EQUIPMENT AND EXPERIMENTAL PROCEDURE

3.1. Introduction

The specimens used in this work were obtained by forging, quenched and then case hardenend until the depth of 1 mm. The material is close to 38CrMo5 and then shot peened with cut wire in rotary chopper wheel equipment.

The dimensions of the gears are of 115 mm diameter and 15 mm width, the analysed part, as can be seen in the figure 13. The material of the gears is a low alloy steel, with the following percentual and average constitution of the major alloying elements:

Table 1 - Major alloying elements in the material composition.

Element	Carbon (C)	Manganese (Mn)	Cromium (Cr)
%	0,17	0,714	0,848

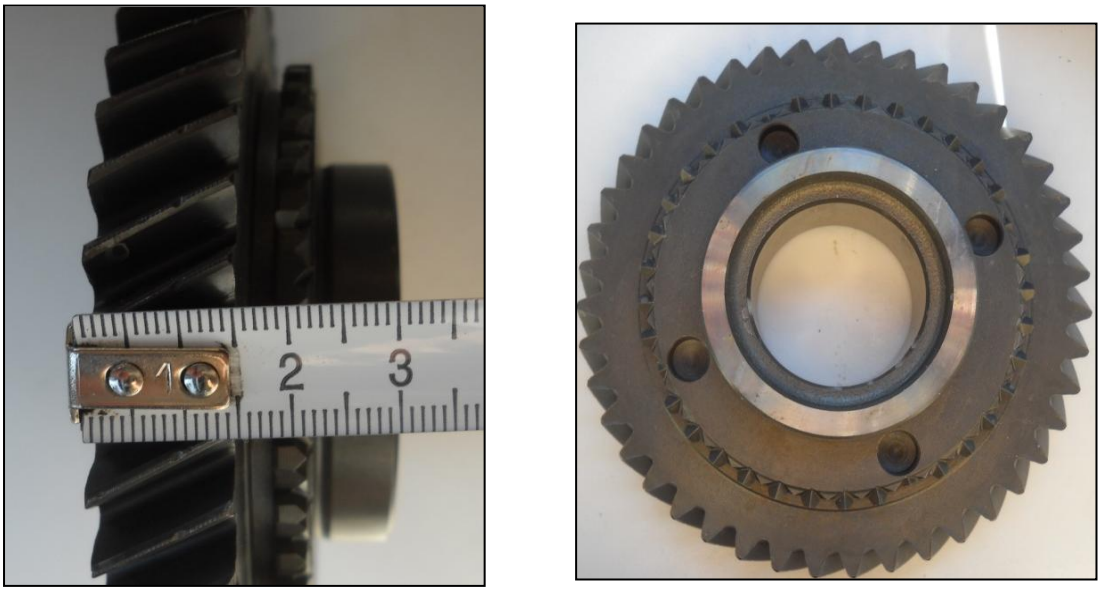

Figure 13 -Original gear from where the several specimens were removed.

3.2. Metallographic Investigations

3.2.1. Sample Preparation

The samples for residual stress measurement were cut with a blade which had aluminium in its composition, so that no more addicional residual stresses are produced in the samples and with a cooling system incorporated so that no alterations on the microstructure are made. In the first gear, the teeth removed are the ones with a red point on top, as it can be seem on the following picture.

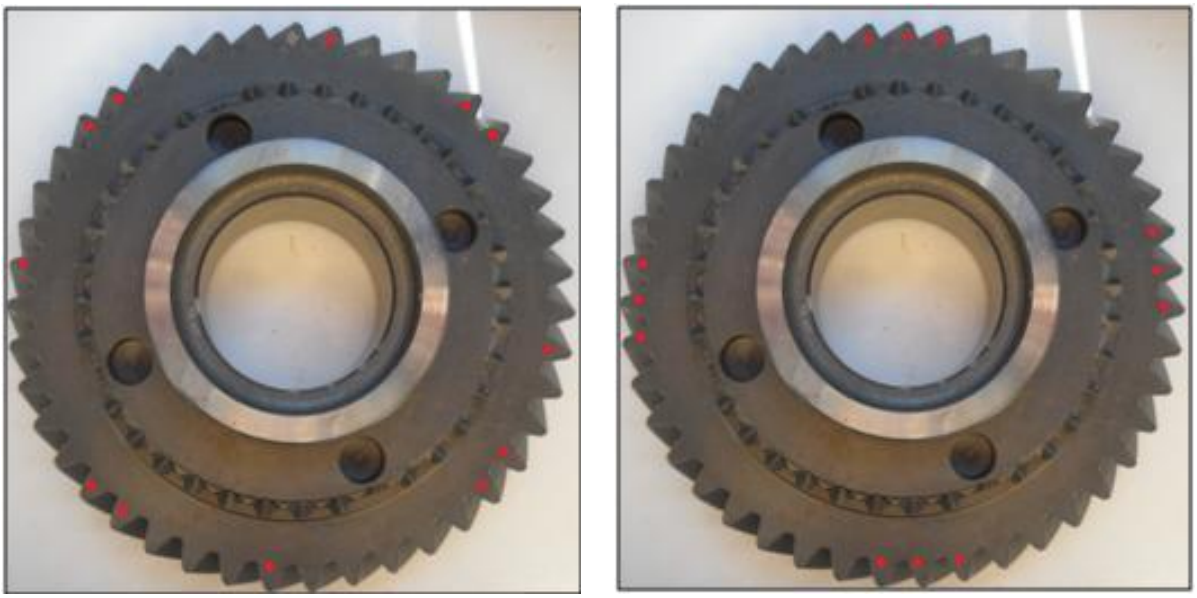

Figure 14 - Teeth removed from the gear number 1, on the left, and teeth removed form the second gear, on the right, both in red.

The measuring point was already specified (1mm above the root fillet and in the centre of the tooth). The sample had to be well positioned, otherwise the X-Ray machine would measure other stresses than in the specified point, as shown in the figure underneath.

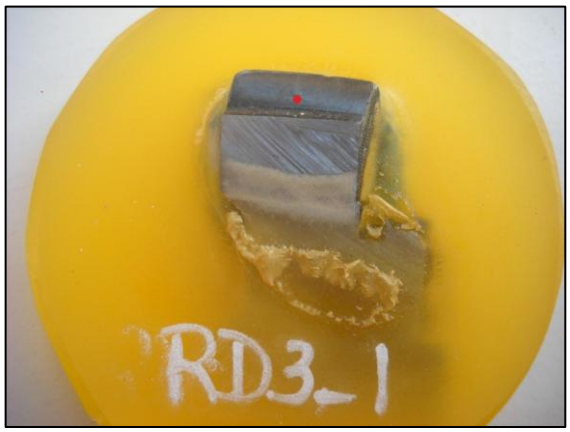

Figure 15 - Samples used for X-ray analyses and measuring point (in red).

To measure the residual stresses, several teeths from the two gears were cut, from the positions 0º, 90º, 180º and 270º with a saw blade, without damaging the surface that would be measured. To be placed in this yellow resin, the sample had to be fixed in a metal plate covered with some vasiline and fixed with plasticine so that the point in red, with the help of a comparator, is the lowest point in a 90º in the horizontal and vertical direction. Several surfaces of the material were measured, such as the surface down to 150 μm, with the help of an electrolyte until the desirable depth. The zone removed was delimited with the help of a hole in a plastic plaque with a certain diameter in the electrolyte machine.

To evaluate the microstructure of the teeth of the gears, they were cut on a 90º angle through the middle. The teeth that were chosen, belonged to perpendicular positions on the gear (0º, 90º, 180º and 270º), corresponding to the same positions where stress measurements were performed in other gears. After the cutting procedure, and to the microstrutural analyses, the samples were embedded in a cylindrical container with epoxy resin grains so that it was possible to move and see them in the microscope. The cylindrical container had a pressure of 300 bar and it had to be warmed so that the plastic grains would melt. The machine had a cooling system to make the plastic harder. Then the edges were smoothed and then the samples were polished in a mechanical equipment and passed through different granulation sandpaper (P320, P600, P1000, P2500) were used in each operation with different times and speeds. Afterwards the samples were polished with a diamond

solution of SPO (colloidal silica polishing suspension with a granulation of 0,02 μm) and finally cleaned in a ultrasonic bath filled with ethanol. The final result can be seen in figure 16, so as the polishing machine.

Figure 16 - Equipment used for sample polishing and samples after being processed in plastic.

3.2.2. Residual Stress Measurement

Residual stress measurements were carried out using X-Ray diffraction technique. The diffractometer chamber is shown in the figure 17.

The diffractometer *D5000* components are a goniometer (1), a detector (2), a detector screen (3), a specimen (4), an adjustable specimen holder in three directions (5), a collimator (6) and a X-ray tube (7). The residual stresses were calculated assuming a plain stress state.

This analysis was combined with an electrolytic material removal technique in order to analyse the stresses in the interior layers of the tooth. The stress relaxations, due to the removal of layers in the material, were not considered.

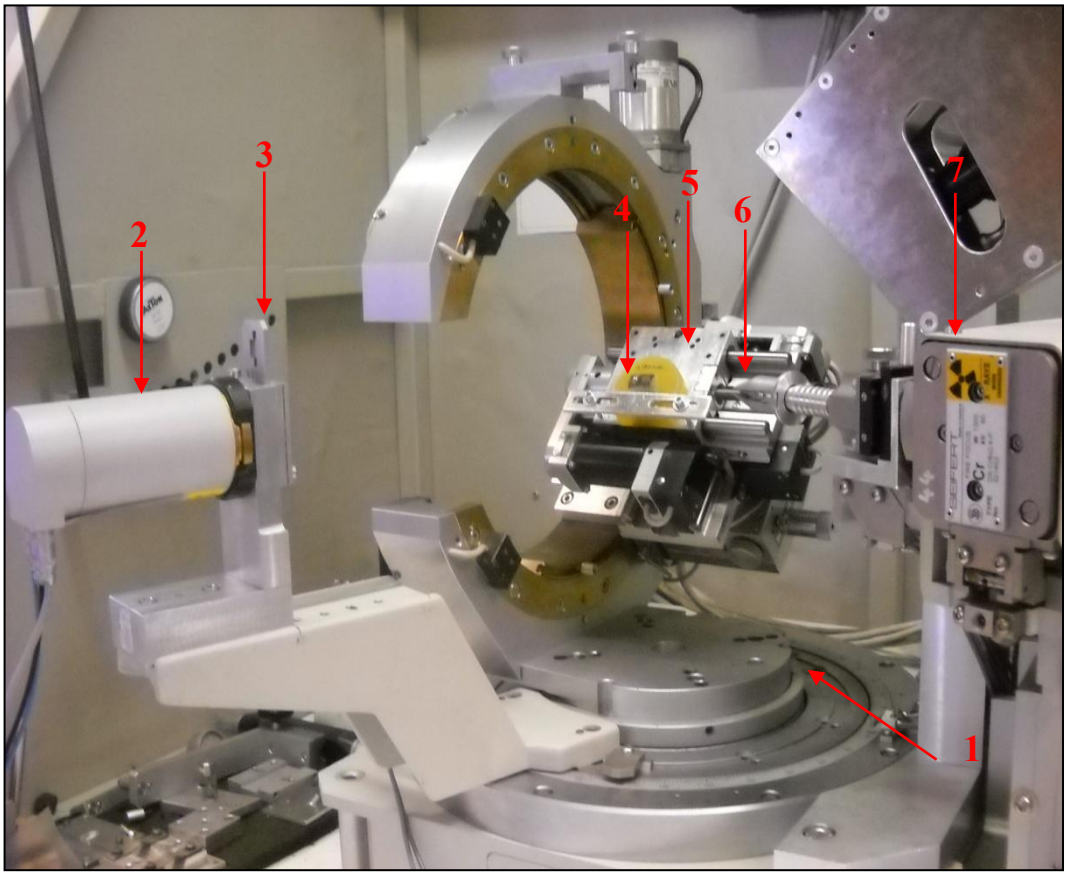

Figure 17 - Schematic representation of the difractometer chamber.

The parameters used for the residual stress measurements are:

Type of radiation:	Cr Kα (chromiun radiation)
Tilting angle:	0º, ±18º, ±27º, ±33º, ±39º, ±45º
Diffraction angle:	$2\Theta_0$ = 156,07º
Diffraction angle range:	148º-164º
Kollimator:	1 mm
Detector screen:	Symmetric slit
Stress determination:	$\sin^2\psi$ method
Line position regulation:	calculated by centre of gravity method
X-ray elastic constant for $\{hkl\}$:	$\frac{1}{2}S^2 = 6,09 \text{ x} 10^{-6} mm^2 / N$

3.3. Hardness tests

The hardness of a metallic material represents its resistance against an indenter penetration. To characterize hardness in metallic materials some tests can be performed and the most common are: Brinell, Vickers, Knoop and Rockwell. All these tests measure hardness by forcing an indenter to penetrate the sample surface. Normally, the indenter is a sphere, pyramid or a cone, made from a material harder than the one tested.

The indenter is normally made of tempered steel, tungsten carbide or diamond. In these tests a certain load is applied to the indenter so that it can penetrate perpendicularly in the material tested surface. After marking the indentation, the indenter is removed, so that it is possible to calculate the hardness value in the plane section or the impression depth.

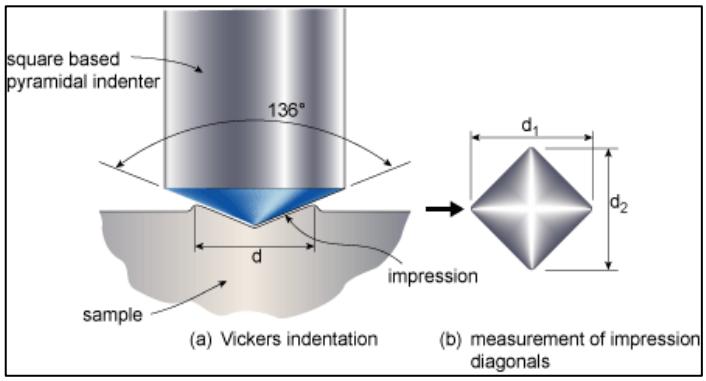

Figure 18 - Schematic representation of Vickers test.

On the right side of this picture it is possible to see the resultant plane section of the Vickers pyramid indentation test in the material sample. This indentation corresponds to a rectangle with edge lengths of d_1. The test accuracy and its sequence followed the norm DIN 50133-1. In this standard it is also possible to find the equation to convert the values measured in the plane surface, into the hardness value in HV (equation 47).

$$HV = \frac{0{,}102F}{A_{contact}} = \frac{0{,}189F}{d_1^2} \tag{47}$$

The equation shows that Vickers hardness is calculated by multiplying one constant by the applied strength and then divided by the value of the contact area. The hardness value is normally indicated according the following standard:

Table 2 - Standard hardness representation.

145	HV	10	/	30
Hardness	Hardness method	Test Load		Duration of the applied load

One of the advantages of the Vickers hardness test applicability is the hide ranges in which it can be used and the fact that it is able to examine even locally structural constituents.

4. EXPERIMENTAL RESULTS

4.1. Evaluation of the depth affected by shot peening

The samples observed at the optical microscope were cut and contained in black plastic according the procedure described in chapter 3, subsection 3.2.1. The removed teeth belonged to the positions of 0º, 90º, 180º and 270º.

After being observed at the optical microscope we could distinguish three different phases within the material: a martensitic phase, a martensitic-bainite phase and a bainite phase, as it is possible to observe in the figure 19.

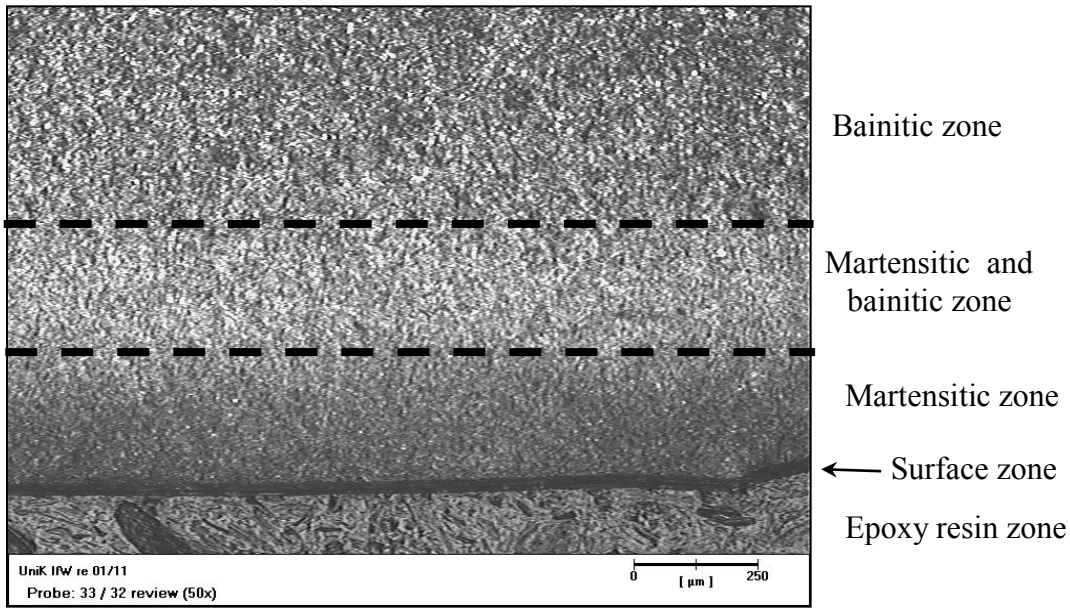

Figure 19 – Microstructure of the surface with a magnifiaction of 50x.

The hardness tests were performed according the procedure described in chapter 3, section 3.3. The following figure shows the indentations performed in longitudinal direction in the flanck area.

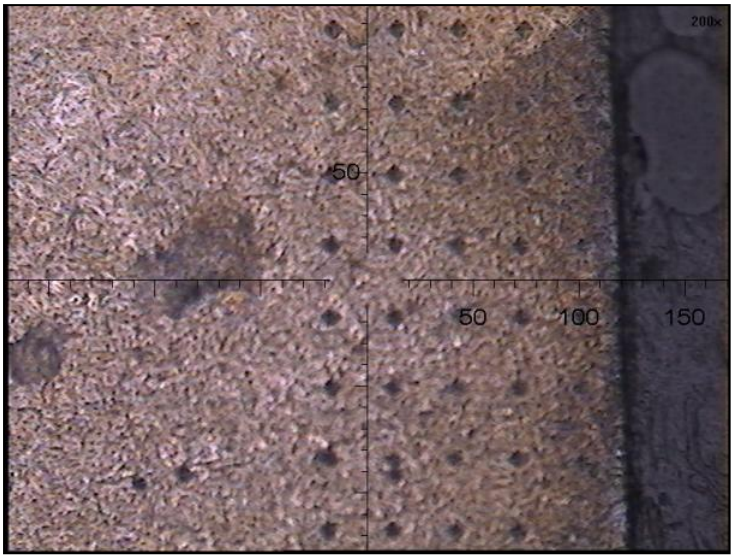

Figure 20 - Hardness indentations with a magnification of 400x

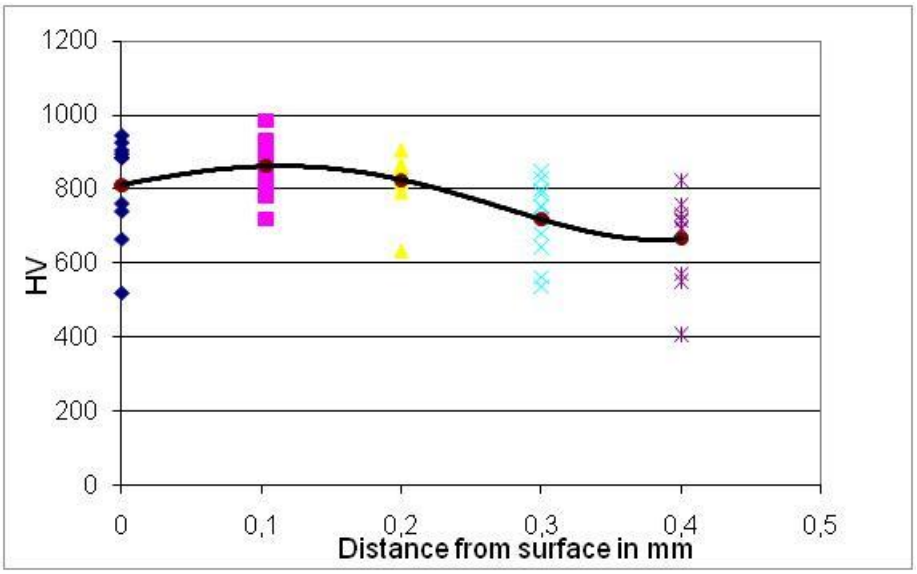

Figure 21 - Relation between distance to the surface and hardness.

The following graphics show the peak width was also measuared along side the residual stresses, as seen below.

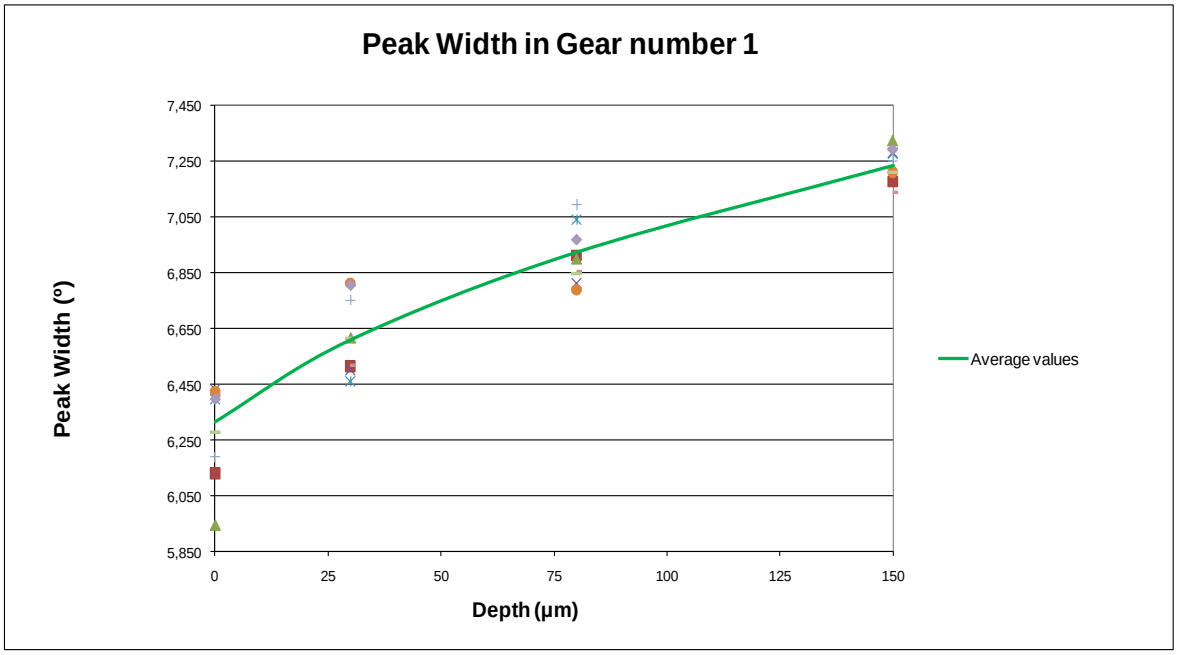

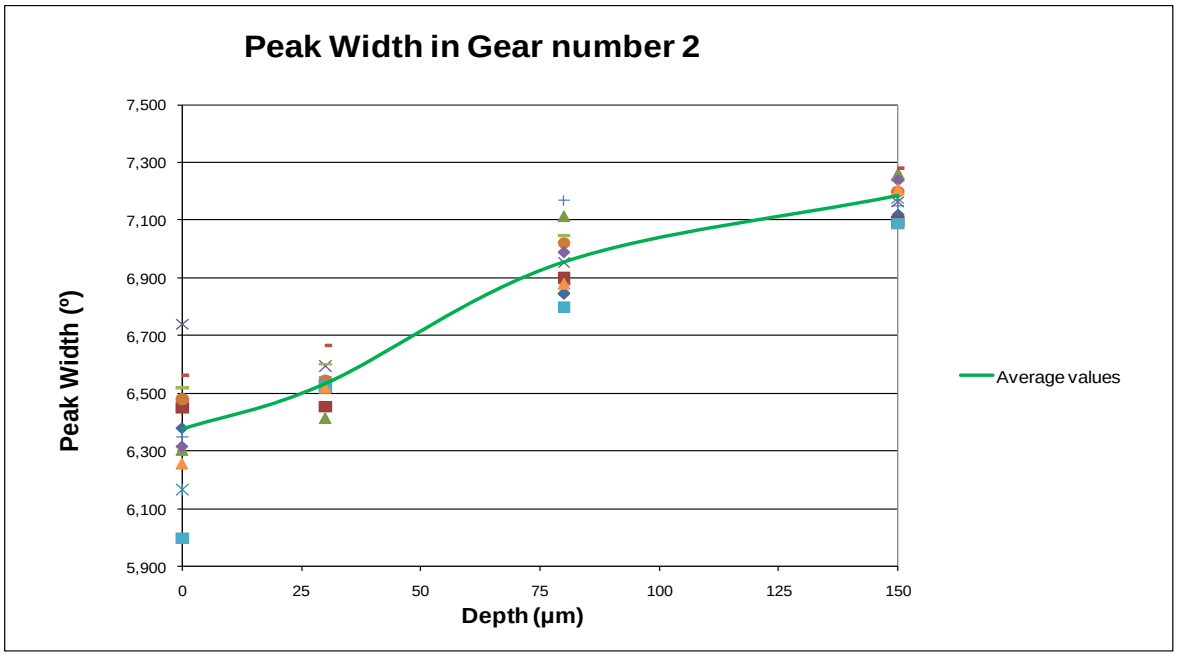

Figure 22 - Peak width distribution with average values, in gears number 1 and number 2. This graphic shows, until the depth of 150 µm, a similar behaviour to the hardness tests results shown in the page before.

4.2. Residual Stress Measurement

The results after the X-ray measurment in 12 specimens in gear number 1 and 12 specimens in gear number 2. The results are displayed in the graphics that follow.

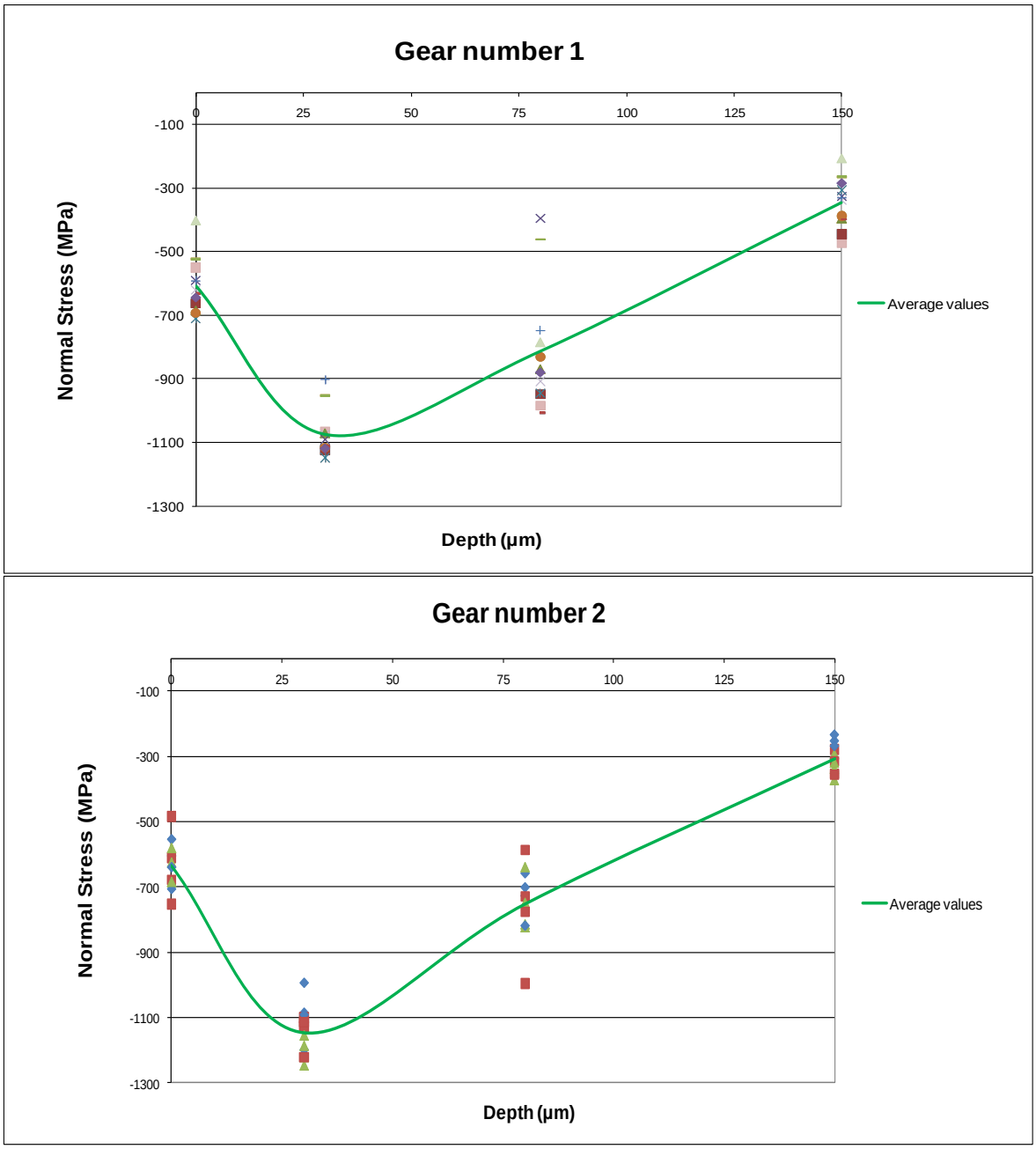

Figure 23 - Representation of the stresses in the first and second analysed gear with correspondent average values

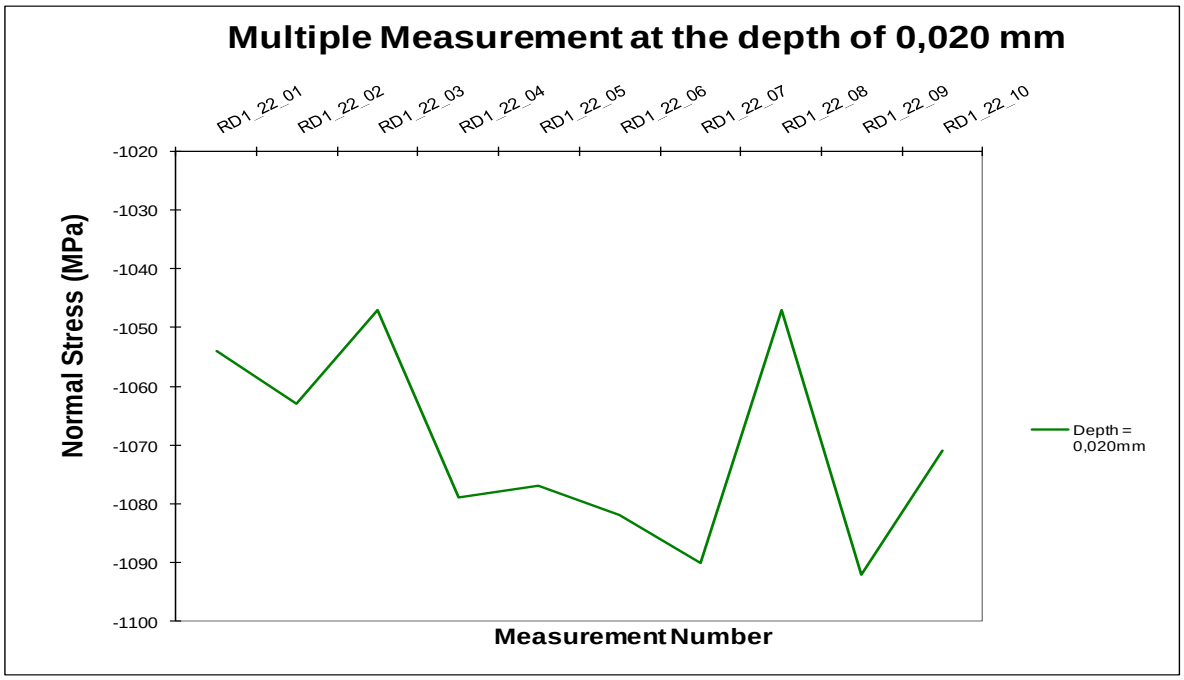

Figure 24 - Series of measurements in the same point with tendency line (6 points).

4.3. Results of the Statistical Tests

For the multiple measurements in the same point the following stress values were observed:

Table 3 - Results for the multiple measurements in one point in the first gear.

Measurement Number	Residual Stress Value [MPa]
RD1_22_01	-1054
RD1_22_02	-1063
RD1_22_03	-1047
RD1_22_04	-1079
RD1_22_05	-1077
RD1_22_06	-1082
RD1_22_07	-1090
RD1_22_08	-1047
RD1_22_09	-1092
RD1_22_10	-1071
Mean Value	-1070,2
Standart deviation	16,74

To these specific values, was applied a Weibull distribution with a 90% confidence interval and the cumulative frequency graphic obtained was the following:

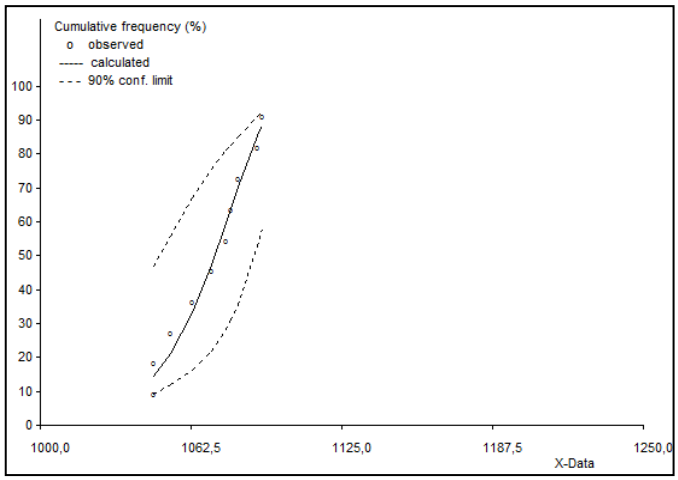

Figure 25 - Weibull cumulative frequency curve using the program CumFreq.

Using a simple linear regression, it was possible to draw the closest line that fitted the values the best.

After treating the values of the measurements in Microsoft Excel®, using the formula "dis.norm(x;media;desvpadr;verdadeiro)" and plotting in the same graphic an empirical distribution function, $\frac{1}{n}$, in which *n* is the number of results that we have, in this case 12. The graphics were plotted to the second and to the first gear analysed and the results are shown in figure 26 to 37:

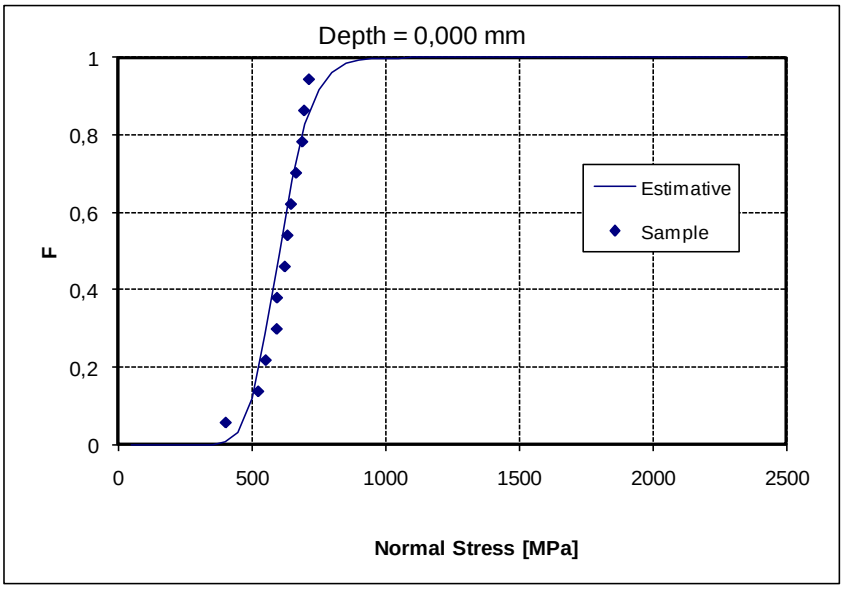

Figure 26 - Normal distribution functions to the depth of 0,000 mm, with a 90% possibility of having a stress value of approximately 492 MPa.

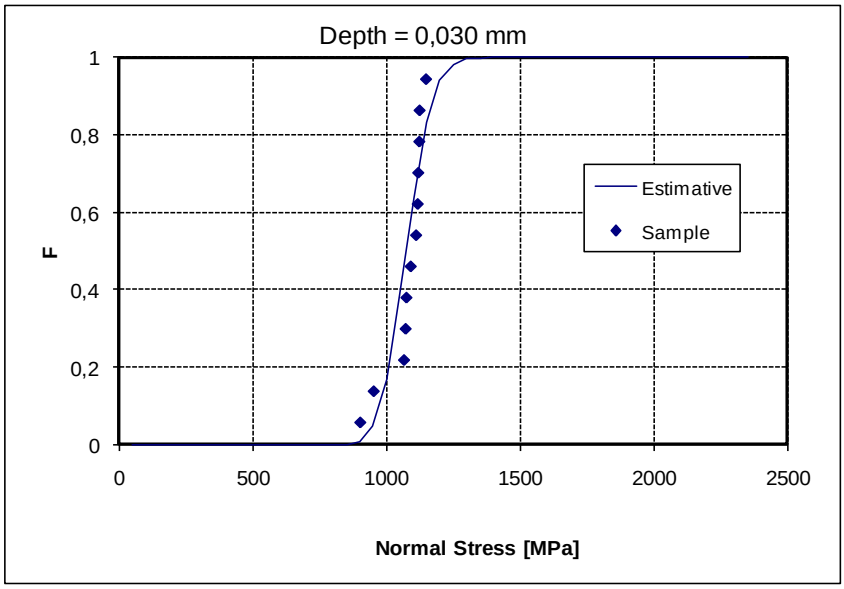

Figure 27 - Normal distribution functions to the depth of 0,030 mm, with a 90% possibility of having a stress value of approximately 978 MPa.

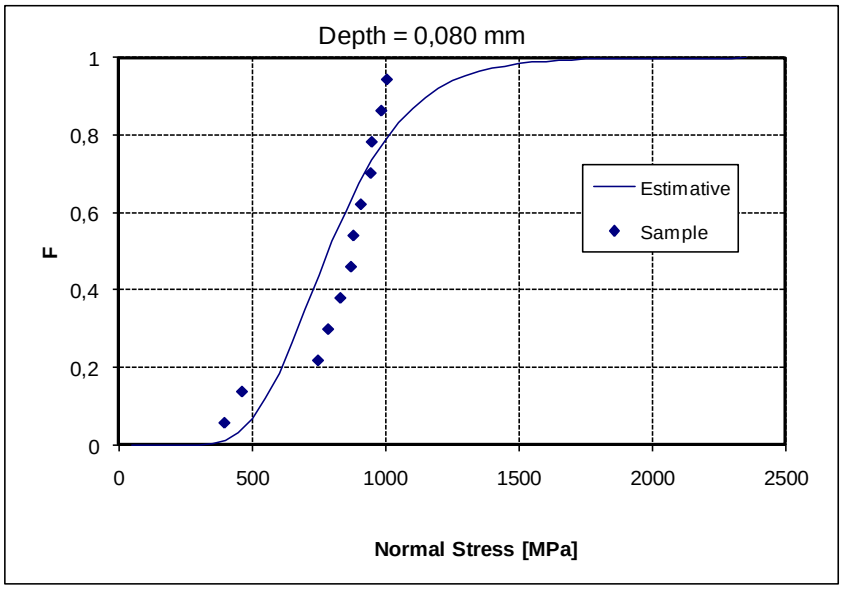

Figure 28 - Normal distribution functions to the depth of 0,080 mm, with a 90% possibility of having a stress value of approximately 535 MPa.

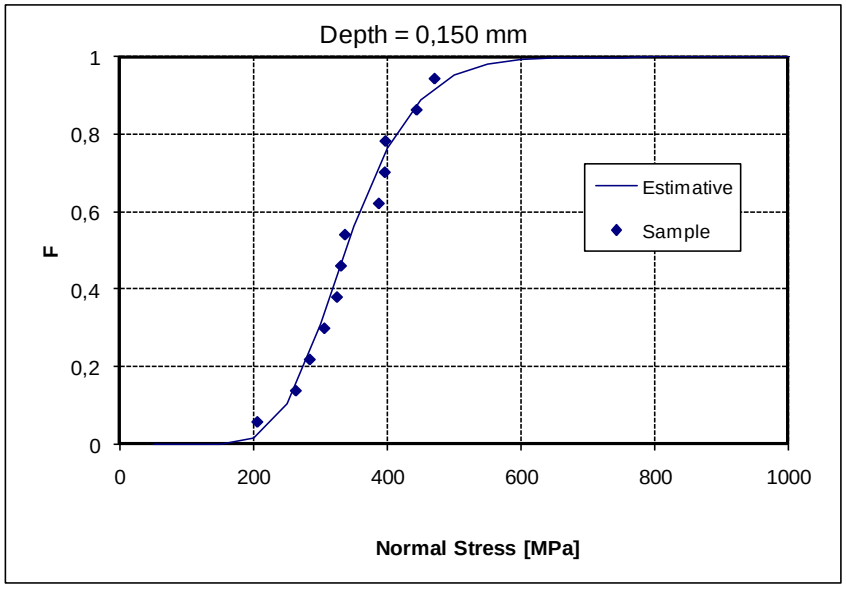

Figure 29- Normal distribution functions to the depth of 0,150 mm, with a 90% possibility of having a stress value of approximately 535 MPa.

Using Microsoft Excel® in order to show the stress distribution around the gear, it was possible to obtain the graphics in the following page for the first gear.

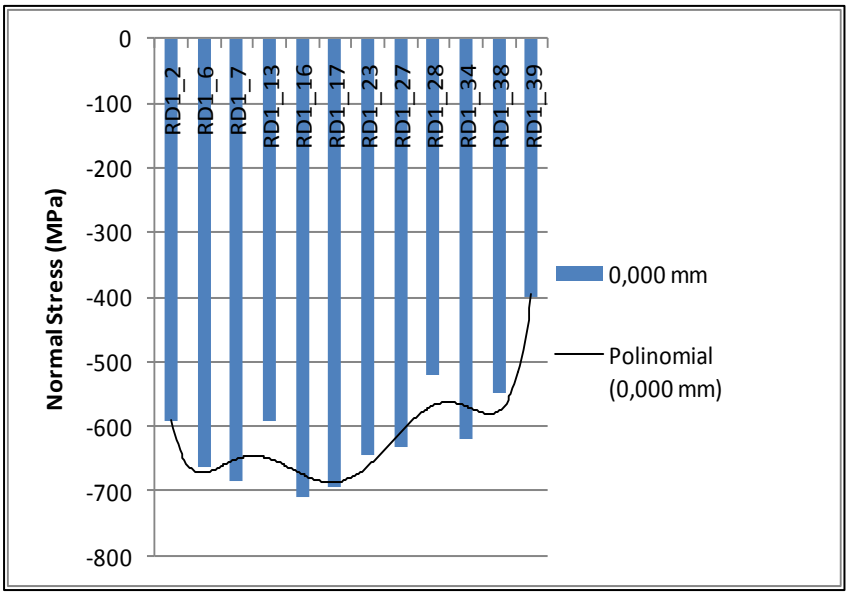

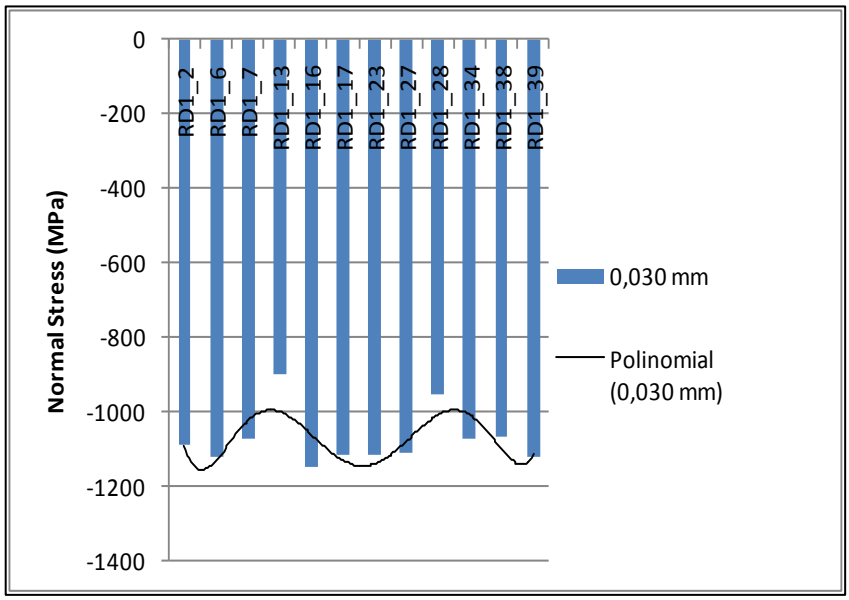

Figure 30 - Normal stress distribution of the first gear for the surface and to the depth of 0,003 mm with tendency line (6 points).

The same procedure was made to the second gear analysed and the graphical results are shown in the following pages.

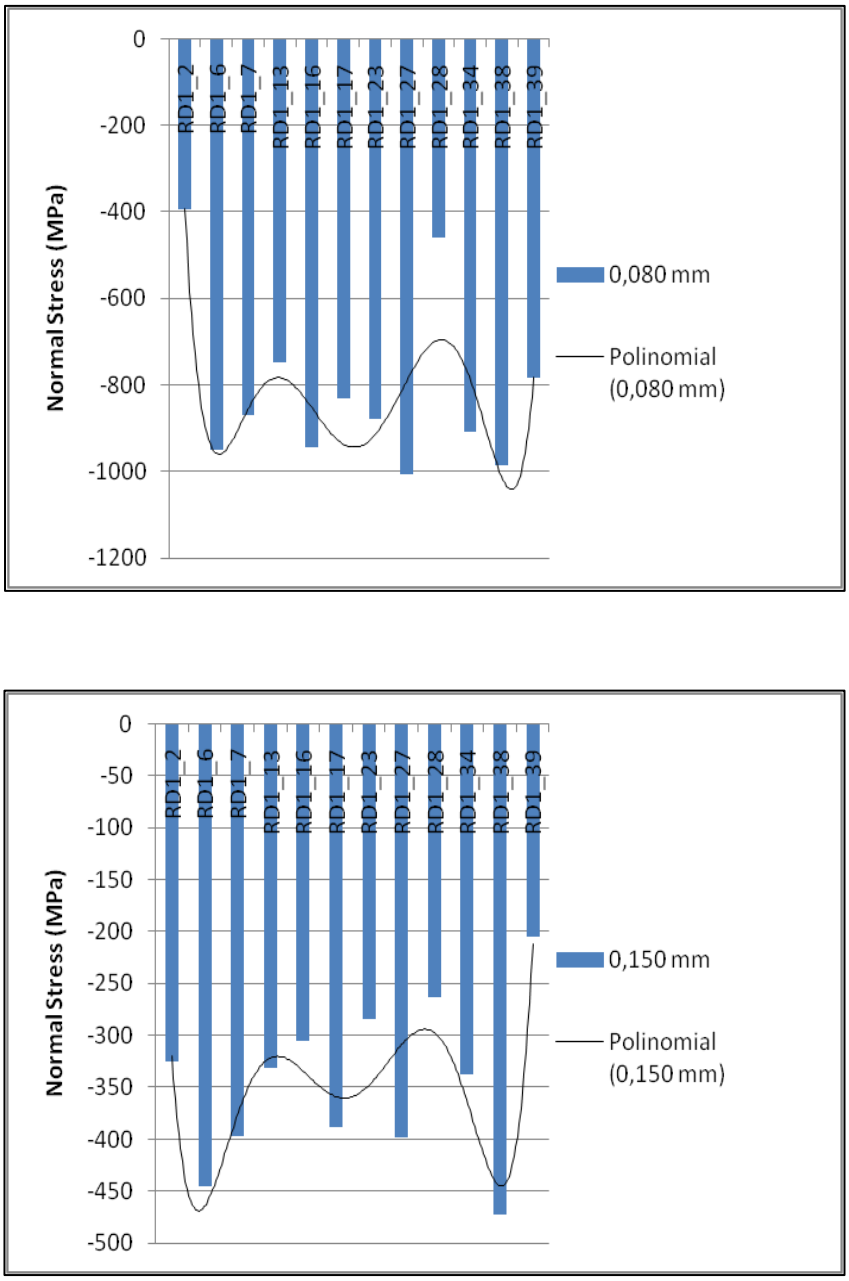

Figure 31 – Normal stress distribution of the first gear for the depths of 0,080 mm and 150 mm with tendency line (6 points).

The graphic results for the second gear are in the following figures.

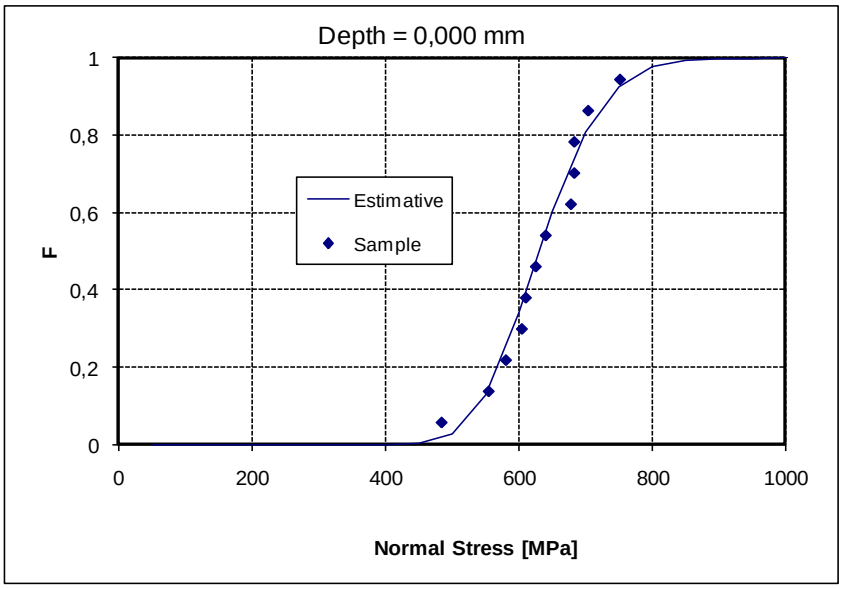

Figure 32 - Normal distribution functions to the depth of 0,000 mm, with a 90% possibility of having a stress value of 590 MPa.

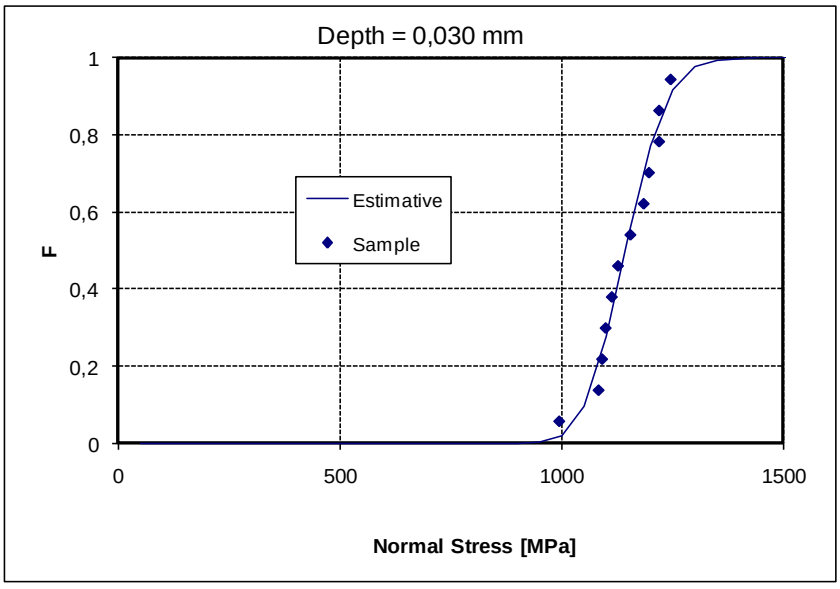

Figure 33 - Normal distribution functions to the depth of 0,030 mm, with a 90% possibility of having a stress value of 1052 MPa.

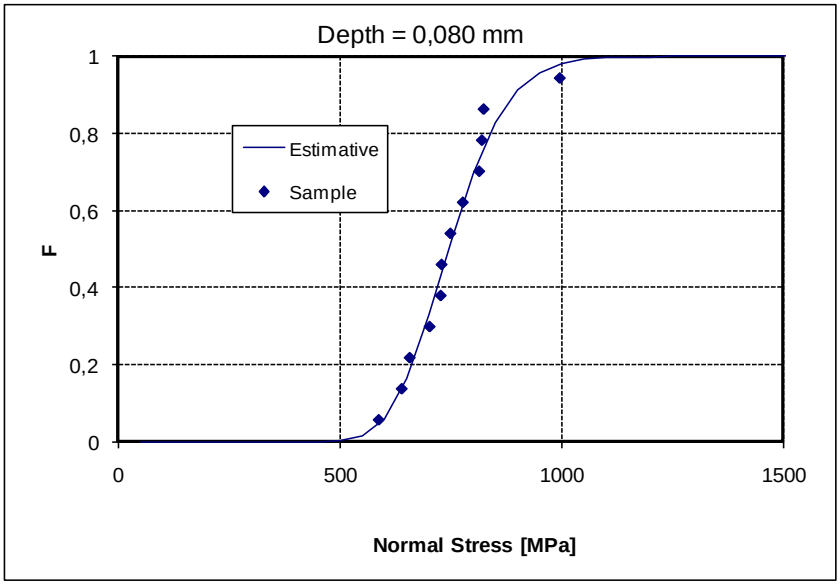

Figure 34 - Normal distribution functions to the depth of 0,080 mm, with a 90% possibility of having a stress value of 623 MPa.

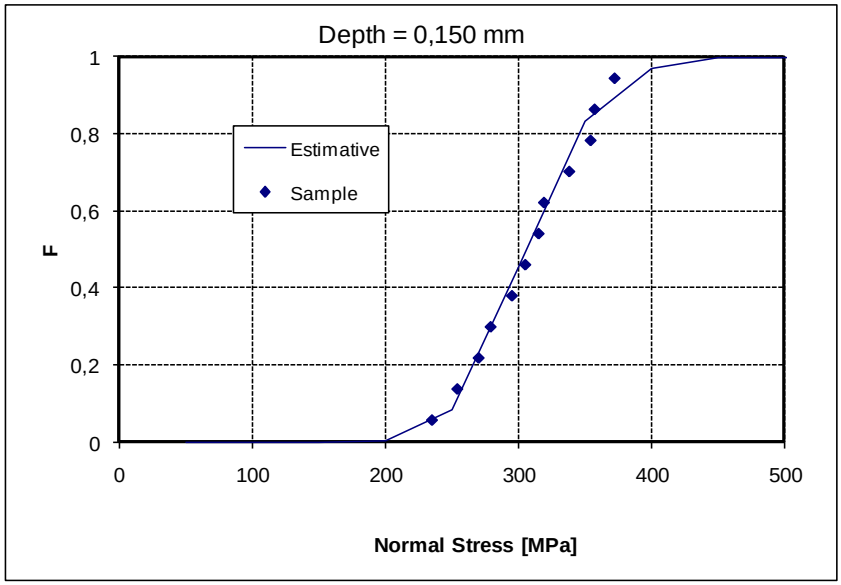

Figure 35 - Normal distribution functions to the depth of 0,150 mm, with a 90% possibility of having a stress value of 254 MPa.

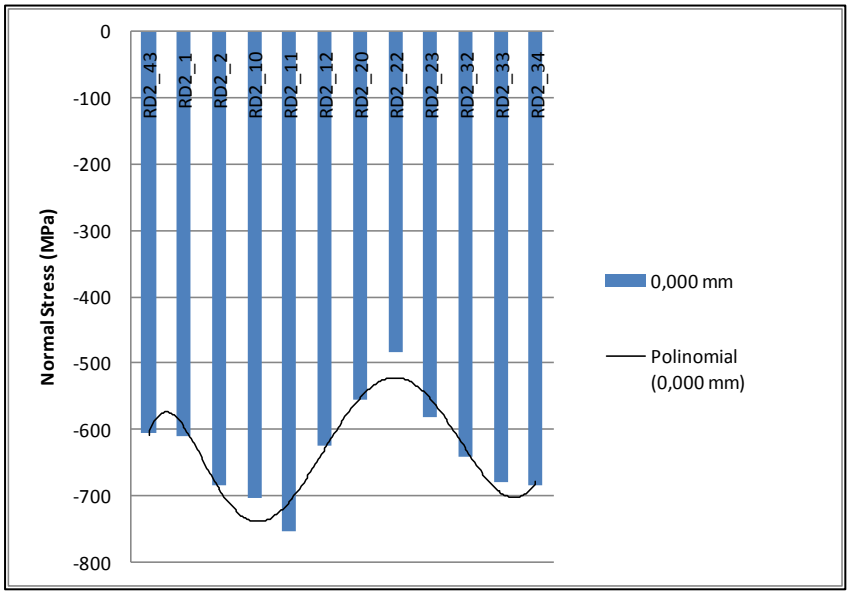

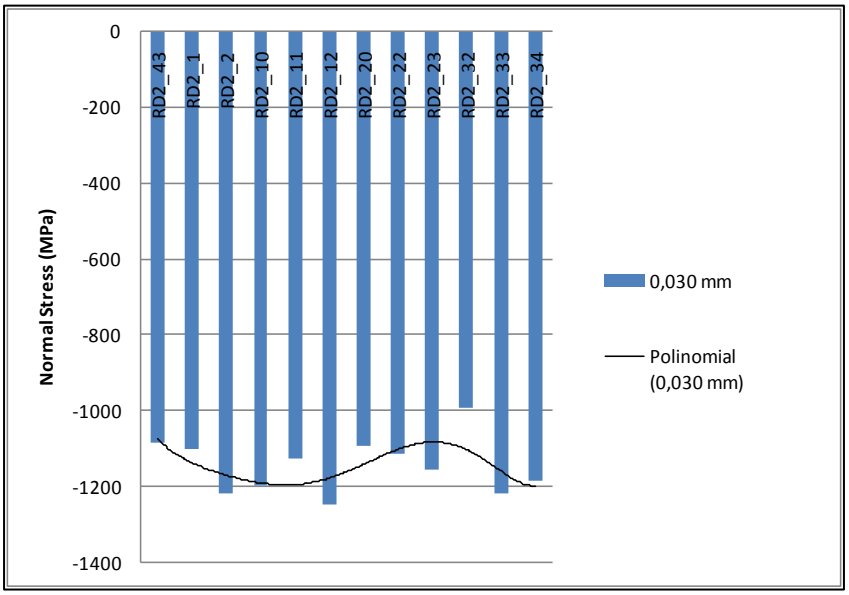

Figure 36 - Normal stress distribution of the second gear for the depths of 0,000 mm and 0,030 mm with tendency lines (6 points).

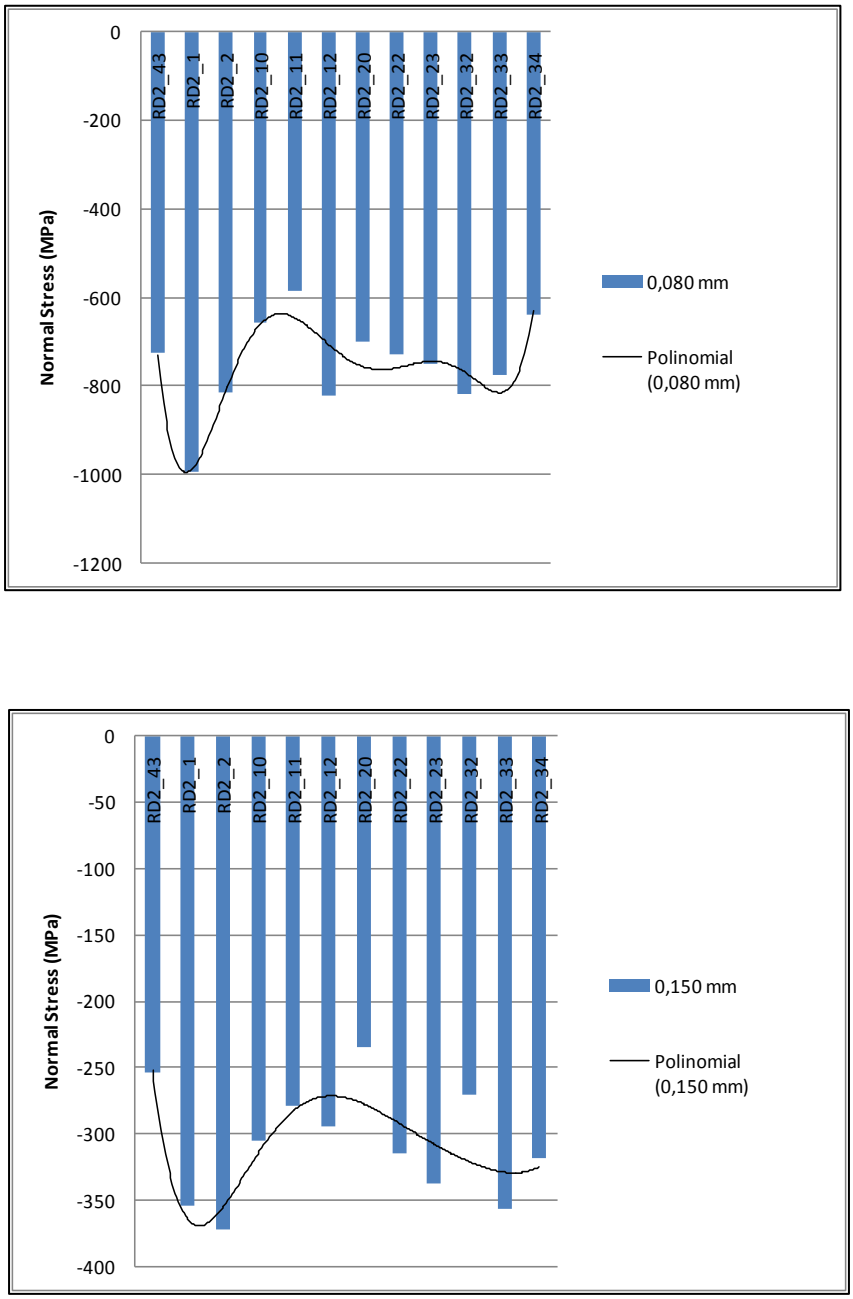

Figure 37 - Normal stress distribution of the second gear for the depths of 0,080 mm and 0,150 mm with tendency lines (6 points).

4.4. Results of the Weibull Analyses

The comparison of the statistical methods are shown for the gears number 1 and number 2.

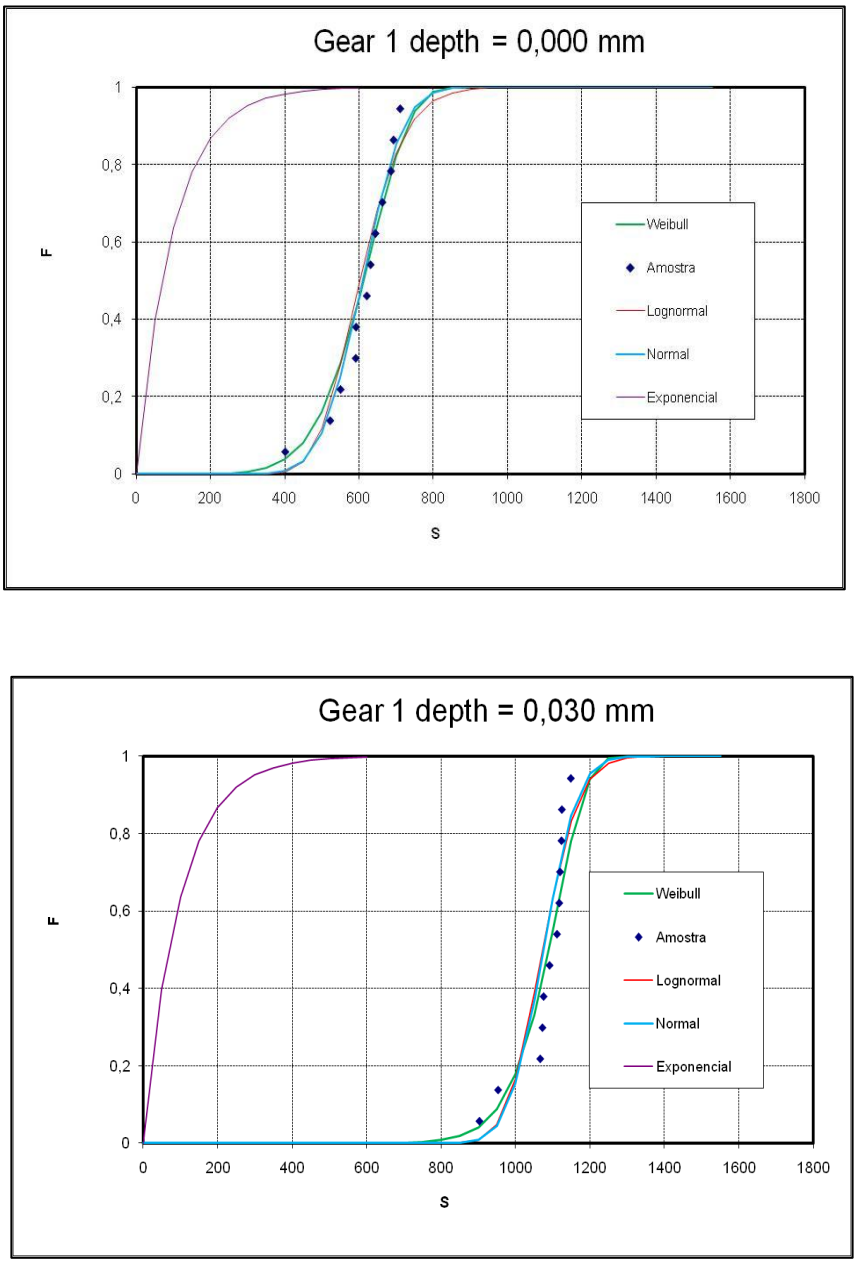

Figure 38 – Comparison between Exponencial distribution, Normal distribution, Log-Normal distribution and Weibull distribution for the depths of 0,000 mm and 0,030 mm, for gear number 1.

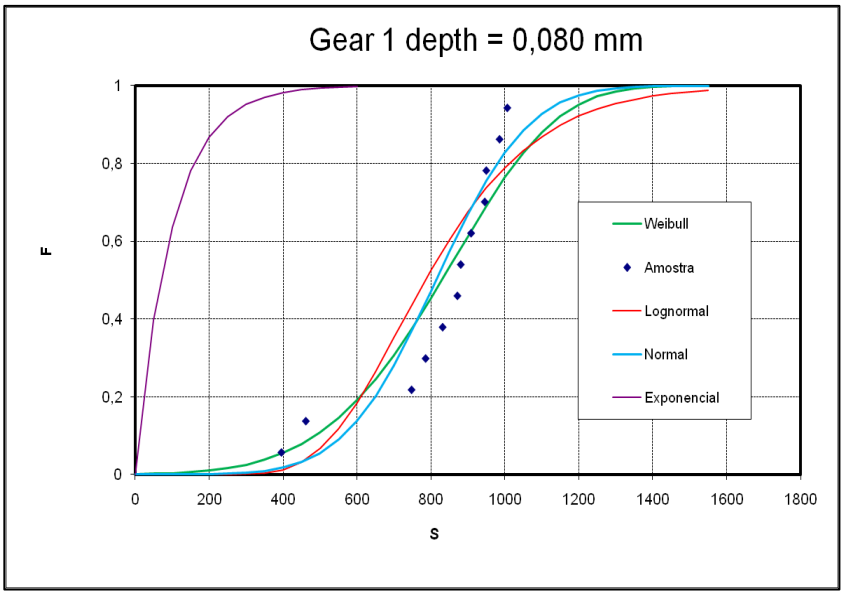

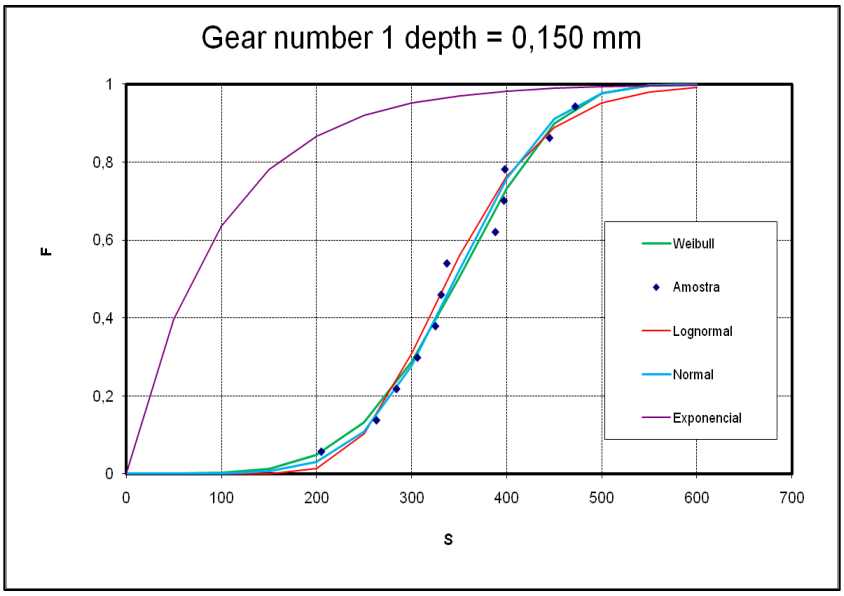

Figure 39 - Comparison between Exponencial distribution, Normal distribution, Log-Normal distribution and Weibull distribution for the depths of 0,080 mm and 0,150 mm, for gear number 1.

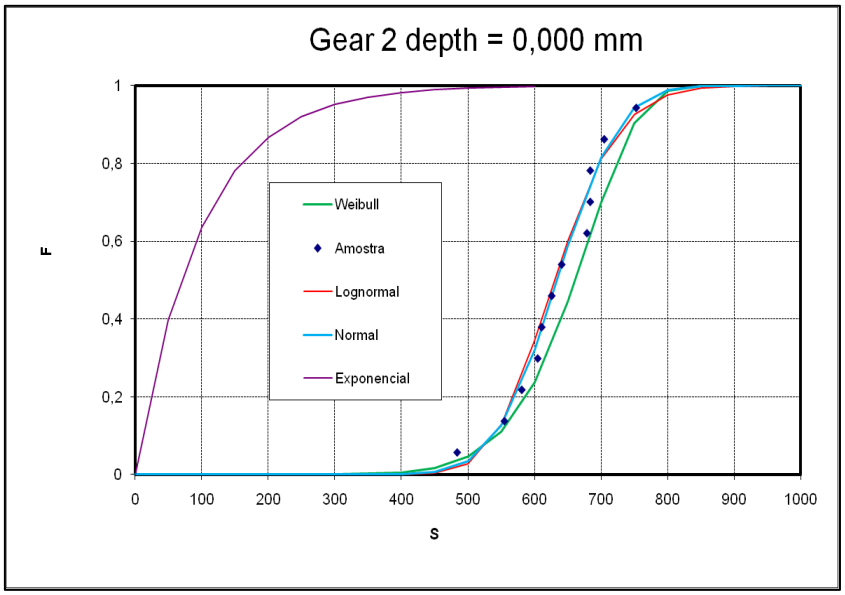
Gear 2 depth = 0,000 mm
F
S
Weibull
Amostra
Lognormal
Normal
Exponencial
0
0,2
0,4
0,6
0,8
1
0
100
200
300
400
500
600
700
800
900
1000

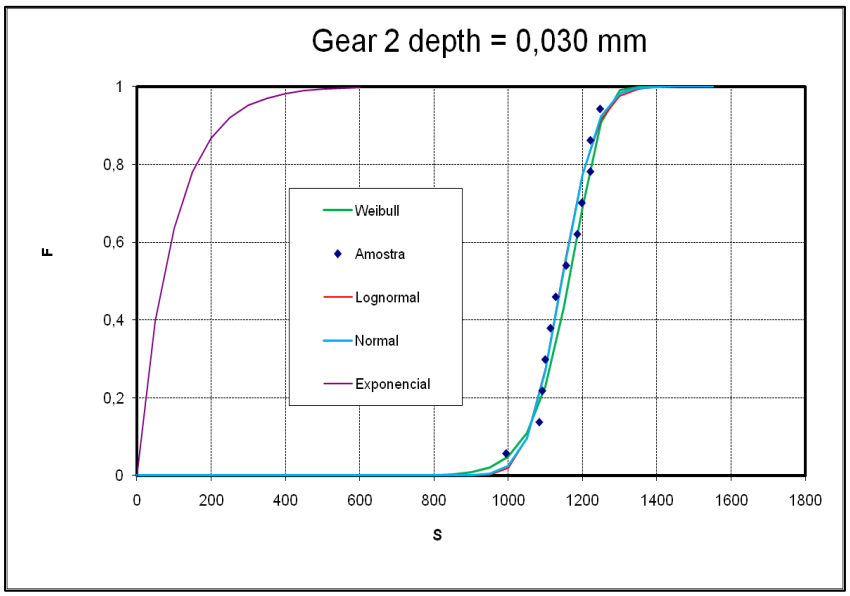
Gear 2 depth = 0,030 mm
F
S
Weibull
Amostra
Lognormal
Normal
Exponencial
0
0,2
0,4
0,6
0,8
1
0
200
400
600
800
1000
1200
1400
1600
1800

Figure 40 - Comparison between Exponencial distribution, Normal distribution, Log-Normal distribution and Weibull distribution for the depths of 0,000 mm and 0,030 mm, for gear number 2.

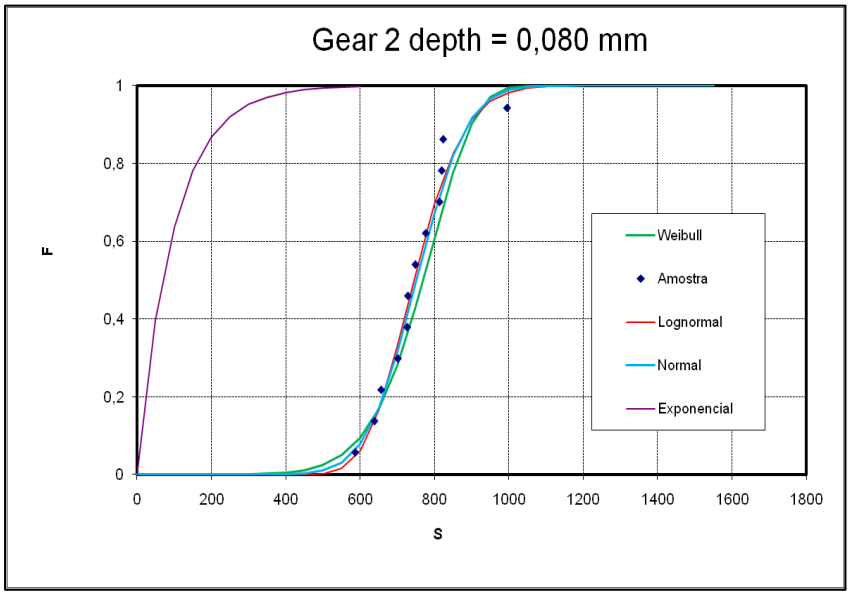

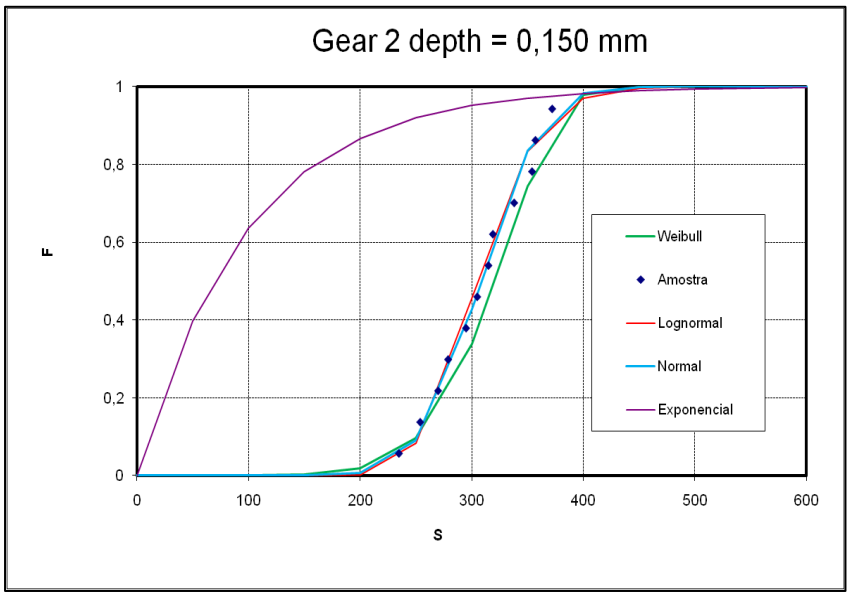

Figure 41 – Comparison between Exponencial distribution, Normal distribution, Log-Normal distribution and Weibull distribution for the depths of 0,000 mm and 0,030 mm, for gear number 2.

5. CONCLUSIONS

After careful consideration and analyses I can take some conclusions from the work that I have developed:

- The maximum compressive residual stress appears, below the surface, between 30 and 50 μm in depth, for both gears.
- The depth affected by the treatment was around 300 μm, as shown by the analysis of in-depth hardness profiles. Hardness values seem to start stabilizing after this depth;
- In the set of multiple measurements, the diference between the maximum and the minimum value was approximately 45 MPa.
- For the first gear, higher differences of the stress level at depths of 80 μm were observed, which also happened in gear number two.
- The peak width values are between, in most of the cases, 6 and 7 degrees. This tells us that the material was case hardened, similar to the information provided by the supplier of the parts, which can also mean that the material has some impurities within the structure;
- In the comparison between the different statistical/probabilistic models, it is possible to observe that all the models fit well the results obtained by X-Ray measurement. The only model that does not is the exponecial model and the one that fits the best is the Weibull model due to its characteristic of being a three

parameter model. Thus, it is possible to adjust better to the results obtained, despite the fact that in some depths the adjustment obtained was not the ideal for the normal distribution.

Finally, the results obtained in this work seems to show that, in future measurements, it is only necessary to remove and analyse one or two teeth from the gears, since the residual stress distribution induced by shot-peening is well described by a normal distribution.

6. REFERENCES

[1] Lee, H.; Mall, Shankar (2003), "Stress relaxation behaviour of shot peened Ti-6Al-4V under fretting fatigue at elevated temperature", Department of Aeronautics and Astronautics, Air Force Institut of Technology (AFIT/ENY), Wright-Patterson AFB, OH 45433-7765, USA

[2] Hoeppner, D.W.; Chandrasekaran, V.; Elliot, C.B. (2000), "Fretting fatigue: Current Techonologies and Practices; ASTM STP 1367, American Society for Testing and Materials, West Conshohocken

[3] Hoeppener, D.; Goss G. (1974), Wear 27 61

[4] Waterhouse, R.B. (1981), R.B. Waterhouse (Ed.) "Fretting Fatigue", Applied Science Publishers, London, pp. 221-240

[5] Leadbeater, G.; Noble, B.; Waterhouse R.B. (1984), S.R. Valluri (Ed.) Proceedings of Sixth Internacional Conference on Fracture, New Delhi, pp. 2125-2132

[6] Mutoh, Y.; Satoh, T.; Tsunoda, E. (1992), M.H. Attia, R.B. Waterhouse (Eds.), Standardization of Fretting Fatigue Test Methods and Equipment, ASTM STP 1159, American Society for Testing and Materials, Philadelphia, pp. 199-209

[7] De Los Rios, E.R.; Trooll, M.; Levers, A. (1999), "Life Extension-Aerospace Techonology Opportunities", The Royal Aeronautical Society Publication, London, pp. 26.1-26.8

[8] Desimone, H.; Bernasconi, A.; Beretta, S. (2005), "On the application of Dang Van criterion to rolling contact fatigue", Politecnico di Milano, Dipartimento di Meccanica

[9] Dang Van, K. (1993), "Macro-micro approach in high-cycle multiaxial fatigue", D.L McDowell, R. Ellis (Eds.), Advances in Multiaxial Fatigue, ASTM STP 1191, Philadelphia, pp. 280-288

Dang Van, K. (2008), "Modelling of damaged induced by contact between solids", Laboratoire de méchanique des solides, UMR 7649 CNRS. École polytechinque, 91 128, France

[10] Dang Van, K.; Griveau, B.; Message, O. (1989), "On a new multiaxial fatigue limit criterion: Theory and applications", M.W. Brown, K.J. Miller (Eds.), EGF 3, Mechanical Engineering Publications, London, pp. 479-496

[11] Peridas, G.; Hills, D.A. (2002), "Crack initiation: the choice of tests available to calibrate Dang Van's criterion", Fatigue Fracture Eng. Mater. Struct. 25 321-330

[12] Lu, J. (1996), "Handbook of Measurement of Residual Stresses", Fairmont Press

[13] François M., Sprauel J.M., Déhan C.F. et al, "X-ray Diffraction Method", Handbook of Measurement of Residual Stresses, Edited by J. Lu, Chapter 5, 1st Ed., SEM, Bethel, pp. 71-131, 1996

[14] Batista A.C., Dias A.M., "Characterization of Mechanical Properties in Surface-Treated Materials", Journal of Testing and Evaluation, Vol. 28, Nr. 3, pp. 217-223, 2000.

[15] Nobre, J.P., (2001) "Sobre o Comportamento Mecânico de Camadas Superficiais dos Materiais: Estudo do Contacto no Impacto Elasto-Plástico e Determinação do Estado de Tensões Residuais pela Técnica do Furo Incremental", Dissertação para a obtenção do Grau de Doutor em Ciências da Engenharia Mecânica, Universidade de Coimbra

7. ANEX A

Gear 1 Teeth 6

Depth	*Normal Stress [MPa]*	*Error*	*Shear Stress [MPa]*	*Error*	*Peak Width [º]*
0,000 mm	-663	33	-43	6	6,424
0,030 mm	-1124	52	-7	10	6,814
0,080 mm	-949	46	-1	9	6,790
0,150 mm	-445	23	-1	5	7,211

Gear 1 Teeth 16

Depth	*Normal Stress [MPa]*	*Error*	*Shear Stress [MPa]*	*Error*	*Peak Width [º]*
0,000 mm	-711	39	-52	7	6,412
0,030 mm	-1148	57	-25	11	6,518
0,080 mm	-945	46	-3	9	6,855
0,150 mm	-306	17	-6	3	7,139

Gear 1 Teeth 27

Depth	*Normal Stress [MPa]*	*Error*	*Shear Stress [MPa]*	*Error*	*Peak Width [º]*
0,000 mm	-651	34	22	6	6,397
0,030 mm	-1111	61	75	12	6,636
0,080 mm	-1006	56	91	11	6,853
0,150 mm	-398	24	53	5	7,222

Gear 1 Teeth 38

Depth	*Normal Stress [MPa]*	*Error*	*Shear Stress [MPa]*	*Error*	*Peak Width [º]*
0,000 mm	-550	31	-36	6	6,131
0,030 mm	-1066	52	-15	10	6,515
0,080 mm	-985	48	-6	9	6,914
0,150 mm	-472	23	19	4	7,177

Gear 1 Teeth 7

Depth	*Normal Stress [MPa]*	*Error*	*Shear Stress [MPa]*	*Error*	*Peak Width [º]*
0,000 mm	-686	39	-69	8	6,398
0,030 mm	-1072	58	-77	11	6,461
0,080 mm	-871	43	-24	8	7,041
0,150 mm	-397	20	0	4	7,278

Gear 1 Teeth 17

Depth	*Normal Stress [MPa]*	*Error*	*Shear Stress [MPa]*	*Error*	*Peak Width [º]*
0,000 mm	-693	38	-47	7	6,278
0,030 mm	-1117	54	-17	10	6,616
0,080 mm	-831	39	9	8	6,849
0,150 mm	-388	18	7	4	7,210

Gear 1 Teeth 28

Depth	*Normal Stress [MPa]*	*Error*	*Shear Stress [MPa]*	*Error*	*Peak Width [º]*
0,000 mm	-552	32	-44	6	6,427
0,030 mm	-953	49	-27	9	6,514
0,080 mm	-461	22	9	4	7,110
0,150 mm	-263	14	19	3	7,202

Gear 1 Teeth 39

Depth	*Normal Stress [MPa]*	*Error*	*Shear Stress [MPa]*	*Error*	*Peak Width [º]*
0,000 mm	-401	23	-31	4	5,944
0,030 mm	-1123	54	29	10	6,617
0,080 mm	-785	43	47	8	6,901
0,150 mm	-205	15	30	3	7,326

Gear 1 Teeth 2

Depth	*Normal Stress [MPa]*	*Error*	*Shear Stress [MPa]*	*Error*	*Peak Width [º]*
0,000 mm	-591	31	-34	6	6,190
0,030 mm	-1091	54	8	10	6,752
0,080 mm	-395	25	27	5	7,095
0,150 mm	-325	19	25	4	7,252

Gear 1 Teeth 13

Depth	*Normal Stress [MPa]*	*Error*	*Shear Stress [MPa]*	*Error*	*Peak Width [º]*
0,000 mm	-592	29	-13	6	6,398
0,030 mm	-903	43	-2	8	6,806
0,080 mm	-747	35	10	7	6,969
0,150 mm	-331	16	11	3	7,292

Gear 1 Teeth 23

Depth	*Normal Stress [MPa]*	*Error*	*Shear Stress [MPa]*	*Error*	*Peak Width [º]*
0,000 mm	-644	37	-55	7	6,350
0,030 mm	-1119	56	-46	11	6,563
0,080 mm	-880	49	54	9	6,904
0,150 mm	-284	14	-4	3	7,239

Gear 1 Teeth 34

Depth	*Normal Stress [MPa]*	*Error*	*Shear Stress [MPa]*	*Error*	*Peak Width [º]*
0,000 mm	-621	32	-24	6	6,431
0,030 mm	-1075	50	0	10	6,503
0,080 mm	-908	48	58	9	6,812
0,150 mm	-377	19	29	4	7,281

Gear 2 Teeth 1

Depth	*Normal Stress [MPa]*	*Error*	*Shear Stress [MPa]*	*Error*	*Peak Width [º]*
0,000 mm	-611	29	-9	6	6,166
0,030 mm	-1100	53	-2	10	6,539
0,080 mm	-996	48	18	9	6,866
0,150 mm	-354	17	11	3	7,174

Gear 2 Teeth 2

Depth	*Normal Stress [MPa]*	*Error*	*Shear Stress [MPa]*	*Error*	*Peak Width [º]*
0,000 mm	-684	34	-18	7	6,479
0,030 mm	-1221	59	21	1	6,545
0,080 mm	-814	40	24	8	7,020
0,150 mm	-372	20	19	4	7,198

Gear 2 Teeth 10

Depth	*Normal Stress [MPa]*	*Error*	*Shear Stress [MPa]*	*Error*	*Peak Width [º]*
0,000 mm	-705	38	-54	7	6,348
0,030 mm	-1198	58	-28	11	6,516
0,080 mm	-657	33	-2	6	7,168
0,150 mm	-305	15	10	3	7,148

Gear 2 Teeth 11

Depth	*Normal Stress [MPa]*	*Error*	*Shear Stress [MPa]*	*Error*	*Peak Width [º]*
0,000 mm	-753	40	-41	8	6,561
0,030 mm	-1128	54	-13	10	6,664
0,080 mm	-587	28	14	5	6,879
0,150 mm	-279	15	24	3	7,279

Gear 2 Teeth 12

Depth	*Normal Stress [MPa]*	*Error*	*Shear Stress [MPa]*	*Error*	*Peak Width [º]*
0,000 mm	-628	31	-12	6	6,520
0,030 mm	-1247	60	22	12	6,600
0,080 mm	-824	40	15	8	7,045
0,150 mm	-295	16	21	3	7,241

Gear 2 Teeth 20

Depth	*Normal Stress [MPa]*	*Error*	*Shear Stress [MPa]*	*Error*	*Peak Width [º]*
0,000 mm	-555	29	-29	6	6,314
0,030 mm	-1092	52	-18	10	6,515
0,080 mm	-702	33	5	6	6,989
0,150 mm	-235	15	15	3	7,239

Gear 2 Teeth 22

Depth	*Normal Stress [MPa]*	*Error*	*Shear Stress [MPa]*	*Error*	*Peak Width [º]*
0,000 mm	-484	26	-27	5	5,998
0,030 mm	-1114	54	10	10	6,522
0,080 mm	-729	38	30	7	6,799
0,150 mm	-315	19	17	4	7,088

Gear 2 Teeth 23

Depth	*Normal Stress [MPa]*	*Error*	*Shear Stress [MPa]*	*Error*	*Peak Width [º]*
0,000 mm	-581	30	-46	6	6,256
0,030 mm	-1156	54	8	10	6,519
0,080 mm	-749	36	-1	7	6,880
0,150 mm	-338	17	3	3	7,208

Gear 2 Teeth 32

Depth	*Normal Stress [MPa]*	*Error*	*Shear Stress [MPa]*	*Error*	*Peak Width [º]*
0,000 mm	-641	34	-8	6	6,380
0,030 mm	-995	48	28	9	6,522
0,080 mm	-820	43	33	8	6,845
0,150 mm	-270	14	15	3	7,119

Gear 2 Teeth 33

Depth	*Normal Stress [MPa]*	*Error*	*Shear Stress [MPa]*	*Error*	*Peak Width [º]*
0,000 mm	-679	34	-11	6	6,449
0,030 mm	-1221	59	-15	11	6,452
0,080 mm	-777	41	26	8	6,899
0,150 mm	-357	18	20	4	7,096

Gear 2 Teeth 34

Depth	*Normal Stress [MPa]*	*Error*	*Shear Stress [MPa]*	*Error*	*Peak Width [º]*
0,000 mm	-684	34	-30	7	6,304
0,030 mm	-1186	59	-30	11	6,414
0,080 mm	-639	30	6	6	7,113
0,150 mm	-319	15	2	3	7,261

Gear 2 Teeth 43

Depth	*Normal Stress [MPa]*	*Error*	*Shear Stress [MPa]*	*Error*	*Peak Width [º]*
0,000 mm	-605	33	-41	6	6,739
0,030 mm	-1084	53	-16	10	6,544
0,080 mm	-727	38	10	7	6,953
0,150 mm	-254	13	7	2	7,164

	Gear 1			
Depth (μm)	0	30	80	150
Residual Stresses	401	903	395	205
	522	953	461	263
	550	1066	747	284
	591	1072	785	306
	592	1075	831	325
	621	1091	871	331
	631	1111	880	337
	644	1117	908	388
	663	1119	945	397
	686	1123	949	398
	693	1124	985	445
	711	1148	1006	472
Average	608,75	1075,17	813,58	345,92
Standart Deviation	79,94	67,85	180,54	71,09

	Gear 2			
Depth (μm)	0	30	80	150
Residual Stresses	484	995	587	235
	555	1084	639	254
	581	1092	657	270
	605	1100	702	279
	611	1114	727	295
	626	1128	729	305
	641	1156	749	315
	679	1186	777	319
	684	1198	814	338
	684	1221	820	354
	705	1221	824	357
	753	1247	996	372
Average	634,00	1145,17	751,75	307,75
Standart Deviation	67,52	67,29	98,64	39,60